

DIPLOMARBEIT

Korrelative Fluoreszenz- und Elektronenmikroskopie zur Untersuchung von Autophagie

Zur Erlangung des akademischen Grades

Diplom-Ingenieurin

Im Rahmen des Studiums

Biomedical Engineering

Eingereicht von

Alina Psenciny

Matrikelnummer 1528589

Ausgeführt am Institut für Angewandte Physik
der Fakultät für Physik der Technischen Universität Wien
in Zusammenarbeit mit BioImaging Austria-CMI

Betreuung

Betreuer/in: Univ. Prof. Dipl.-Ing. Dr. techn. Gerhard Schütz
Dr. Andreas Walter

Wien, 21.07.2018

Alina Psenciny

Gerhard Schütz



TECHNISCHE
UNIVERSITÄT
WIEN

Correlated Multimodal Imaging
BioImaging Austria - CMI

MASTER'S THESIS

**Correlation of Advanced Fluorescence
Microscopy and Transmission Electron
Microscopy to study Autophagy**

To obtain academic degree of
Master of Science

In the course of the study

Biomedical Engineering

By

Alina Psenciny

Matriculation number 1528589

Carried out at the Institute for Applied Physics
of the Vienna University of Technology
in cooperation with BioImaging Austria - CMI

Supervision

Supervisor: Univ.Prof. Dipl.-Ing. Dr.techn., Gerhard Schütz
Dr. Andreas Walter

Vienna, 21.07.2018

Alina Psenciny

Gerhard Schütz

Erklärung zur Verfassung der Arbeit

Alina Psenicny, B.Sc.
Reznicekgasse 10/9
A-1090 Wien

Hiermit erkläre ich, dass ich diese Arbeit selbständig verfasst habe, dass ich die verwendeten Quellen und Hilfsmittel vollständig angegeben habe, dass ich die Stellen der Arbeit, – einschließlich Tabellen, Karten und Abbildungen – die anderen Werken oder dem Internet im Wortlaut oder dem Sinn nach entnommen sind, auf jeden Fall unter Angabe der Quelle als Entlehnung kenntlich gemacht habe.

21.07.2018

Alina Psenicny

Acknowledgments

First of all I would like to express my gratitude to Dr. Andreas Walter, who gave me the opportunity to work on this exciting project and has been the best external supervisor a student can wish for. He was there to help on every step of the way providing me with guidance and suggestions, no matter the question or the hour. I would also like to express my deepest thanks for Christian Loeffke, Edmundo Ricardo Sanchez Guajardo, Stephan Handschuh, Nicole Fellner, Harald Kotisch, Marlene Brandstetter, Sonja Jacob and Thomas Heuser. They have been nothing but helpful and I would have not come as far as I did without their support (professional as with some, personal). They assisted me when I was stuck and gave me motivation to proceed and not give up. I would also like to thank my partner in crime or battle against autophagosomes, Tamina Laimer. She had to listen to me talking about the exciting progress and discouraging obstacles from the beginning of our autophagy journey and if it would not have been for her, who would I have turned to during those coffee hours?! My parents have always been there for me, and during this study they have been my rock. My sisters Evita and Ilana always found the best way to cheer me up and brighten my days. Big thanks go to the family I chose, Katharina Keuenhof, who kept me whole and without whom I would have not dealt with this year as well as I did. Jakob Schneider, no words are enough or needed, as you know (and are) everything.

Zusammenfassung. Heutzutage sind Wissenschaftlern viele verschiedene bildgebende Verfahren verfügbar, dennoch ist es nach wie vor eine Herausforderung diese adäquat zu kombinieren um biologische Fragestellungen ganzheitlich zu beantworten und den gesamten relevanten Auflösungsbereich zu nutzen. Die Kombination verschiedener bildgebender Verfahren wird Correlative Imaging genannt: Informationen über die zu untersuchende Probe werden durch mindestens zwei komplementäre Verfahren gesammelt, die eine ganzheitliche Ansicht der Probe erzeugen. Dadurch können komplementäre Informationen über Struktur, Dynamik, Funktion und molekulare Komposition derselben Probe geliefert werden. Das Ziel dieses Projektes war es, eine multimodale korrelative Imaging Pipeline zu entwickeln und Autophagie in Pflanzen zu untersuchen. Mit dieser Pipeline wurde in-vivo proteinspezifische Information über Autophagosome in wachsenden Wurzelspitzen von Arabidopsis in Kontext mit deren Ultrastruktur gesetzt. Die Pipeline ermöglicht es, einen Überblick über Autophagosome in deren natürlicher 3D Umgebung zu erhalten (Autophagieatlas von Wurzeln), deren zellspezifisches Auftreten zu beurteilen und in Folge bis zur Ultrastruktur heran zu zoomen um die Verteilung innerhalb der Zellen mit einer Nanometer-Genauigkeit zu visualisieren, um deren Ursprung und das Areal der Biogenese zu erforschen. Um den Autophagie Atlas zu visualisieren wurde konfokale Spinning-Disk-Mikroskopie, Lichtscheibenmikroskopie und micro-Computertomographie (μ CT) genutzt. Der zelluläre Kontext der Autophagosomen wurde durch Verwendung von Transmissionselektronenmikroskopie dargestellt. Hochdruckgefrieren wurde genutzt um den möglichst natürlichen Zustand der Wurzel direkt nach dem in-vivo Imaging zu fixieren und zu präservieren. Die Entwicklung dieses multimodalen Workflows erforderte die Optimierung der Probenvorbereitung um Kompatibilität zwischen den verschiedenen Techniken zu gewährleisten. Dieser

neuartige Workflow, der in dieser Arbeit präsentiert wird, ermöglicht es in eine intakte Probe heranzuzoomen – angefangen von ihrer gesamten 3D Morphologie bis hin zu ihrer Ultrastruktur – was genutzt werden kann um eine Vielzahl von gegenwärtigen Fragestellungen zu untersuchen.

Abstract. Many imaging modalities are available to scientists nowadays, nevertheless it remains a challenge to combine them adequately to answer the biological research question of interest holistically and resolve all relevant length scales. The combination of modalities for the examination of a single specimen is termed correlative imaging: Information about the specimen is gathered with two or more complementary modalities which create a composite view of the sample. This view can provide complementary information about structure, dynamics, function and molecular composition of a single specimen. My main goal was to develop a multimodal correlative imaging pipeline to study autophagy in plants. With this pipeline, in-vivo protein-specific information about autophagosomes within growing *Arabidopsis* root tips was placed into its ultrastructural context. The pipeline allows to acquire an overview of autophagosomes within their native 3D environment (autophagy atlas of roots), assess their cell-specific occurrence and zoom in on their ultrastructural distribution within single cells with nanometer precision to study their origin and area of biogenesis. To visualize the autophagy atlas confocal spinning disk microscopy, light sheet microscopy and Micro-Computed Tomography (μ CT) were used. The cellular context of the autophagosomes was visualized using Transmission Electron Microscopy. High-pressure freezing was used to fix and preserve the near-native state of the root right after in-vivo imaging. The development of this multimodal workflow required optimization of sample preparation to ensure compatibility between the techniques. The novel workflow presented in this thesis allows to zoom in on an intact sample starting from its overall 3D morphology down to its ultrastructural composition, which can be used to explore a multitude of current research questions.

Contents

1	Introduction	4
2	Motivation.....	8
3	Theoretical Framework.....	10
3.1	Confocal Microscopy (CM)	10
3.1.1	Principles of CM.....	11
3.1.2	Spinning disk confocal microscopy (SDCM).....	14
3.2	Light Sheet microscopy (SPIM).....	14
3.2.1	Principles of SPIM.....	15
3.3	Micro-computed tomography (μ CT).....	17
3.3.1	Principles of μ CT.....	18
3.4	Transmission Electron Microscopy (TEM)	19
3.4.1	Principles of TEM.....	20
3.5	Correlative Light and Electron Microscopy (CLEM).....	23
3.6	Near-Native Sample Fixation.....	25
3.6.1	High Pressure Freezing (HPF)	25
3.6.2	Freeze substitution (FS)	28
3.7	Biological Background	29
3.7.1	Autophagy.....	29
3.7.2	Autophagy in <i>Arabidopsis</i> roots	31
4	Materials and Methods.....	34
4.1	Correlative workflow.....	34
4.1.1	Light microscopy and sample preparation.....	35
4.1.2	Chemical fixation.....	39
4.1.3	High Pressure Freezing	40
4.1.4	Freeze substitution and embedding	41
4.1.5	Sectioning.....	45
4.1.6	CLEM	46
4.1.7	Post-Staining and imaging with TEM.....	47
5	Results.....	49

5.1	Imaging modalities.....	49
5.1.1	SPIM.....	49
5.1.2	CM.....	51
5.1.3	SDCM.....	53
5.1.4	μ CT.....	55
5.1.5	TEM.....	56
5.2	Correlating modalities.....	61
5.2.1	SDCM, CLEM and TEM.....	62
5.2.2	SDCM, μ CT and TEM.....	63
5.2.3	SPIM, μ CT and TEM.....	64
6	Conclusion.....	66
7	Outlook.....	69
8	Bibliography.....	70

List of Abbreviations

AFS for Automated Freeze Substitution device
ATG for Autophagy-related
BSA for Bovine Serum Albumin
CFSEM for Correlative Fluorescence Scanning Electron Microscopy
CFTEM for Correlative Fluorescence Transmission Electron
Microscopy
CLEM for Correlative Light and Electron Microscopy
CM for Confocal Microscopy
CT for Computed Tomography
EM for Electron Microscopy
FS For Freeze Substitution
GFP for Green Fluorescent Protein
HPF for High Pressure Freezing
LM for Light Microscopy
PBS for Phosphate Buffered Saline
SDCM for Spinning Disk Confocal Microscopy
SEM for Scanning Electron Microscopy
SPIM for Single Plane Illumination Microscopy
TEM for Transmission Electron Microscopy
UA for Uranyl Acetate
 μ CT for Micro-Computed Tomography

1 Introduction

A human eye can see objects as small as 0.1 mm. When a device can undercut this distance – resolution (resolving power) – we call it a microscope. In history various microscopy techniques have been developed, starting with light microscopes. Their maximal resolution is given by the equation:

$$\delta = \frac{(0.61\lambda)}{NA} \quad (1)$$

where λ is the wavelength of the radiation and NA the numerical aperture of the microscope's objective with equation:

$$NA = n\sin\theta \quad (2)$$

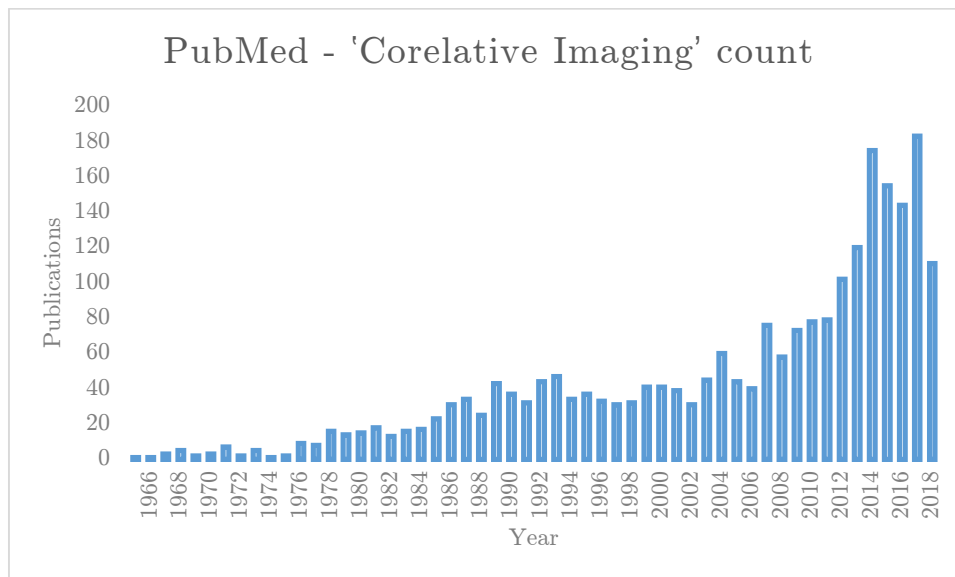
with θ being the half angle of the maximal cone of light entering and exiting the lens and n being the refractive index of the substance between the lens and sample. For instance, the lowest visible violet light to humans which has a wavelength of approximately 380 nm and a microscope with a numerical aperture of 1.3, gives us a resolution of 178 nm. Although that is small to the human eye, it still corresponds to the size of about a thousand atoms. For a long time in history, it was not possible to resolve anything smaller than the wavelength of light. This excluded a large group of objects on single molecule level from observation using classical light microscopy (LM), e.g. viruses, DNA, proteins, smaller molecules and atoms. Thus, there was an urgent need for a technique that is able to resolve structures at a higher resolution. In 1932, the first description of an electron microscope (EM) was made by Knoll and Ruska.

Usually, not all information crucial to an answer is present within one image. It is of utmost importance to fully understand the dynamics and temporal scales of an organism and to understand how its molecular machinery operates. This is how correlative microscopy was born. The idea has been around for more than 50 years and the phrase correlative microscopy was first mentioned in 1969 in a paper from McDonald & Hayes [1], referring to the correlation of light and electron

microscopy. It was only five years later that Geissinger et al. [2] published a protocol for imaging the same region of interest in the same sample using both techniques.

The success of the method opened doors for many new possibilities and combinations to be explored. Various techniques have already been paired, including clinical imaging modalities and different kinds of microscopy.

Correlative imaging is becoming more and more important in the last few years, as seen in Graph 1, where the number of publications found on PubMed when searching for 'Correlative imaging' are represented for the last 54 years with a peak of 183 publications in 2017.



Graph 1 Timeline of publications found on PubMed for 'Correlative Imaging'. First publication was found in year 1964 and the number of publications has grown to highest in the year 2017, when 183 publications were published.

Correlative imaging was found suitable for this project. The object of our study was autophagy in root tips of *Arabidopsis thaliana*, and our goal was to develop a multimodal pipeline to combine protein-specific information about autophagosomes within growing root tips with information about their ultrastructural context. Correlating advanced LM and Transmission Electron Microscopy (TEM) was

found to be the best fit. Advanced LM in combination with green fluorescent protein (GFP) and its ability to genetically label cellular proteins, like ATG8 proteins in *Arabidopsis* roots, provides the unique possibilities to observe processes within the living root over time and to place them into the cellular context, providing us with behavioural information about specific proteins. A bigger field of view over several cells is useful for determining the location of autophagosome formation within the root, but in order to look in deeper and study the intercellular location, these techniques do not provide a sufficient resolution. In contrast, TEM provides intercellular information at a nanometre resolution. A near-native sample preservation is crucial for all imaging modalities. In order to visualise the sample in a state that most resembles its physiological one with TEM, the morphology and ultrastructure should remain unchanged and the structures of interest should remain clearly marked. High pressure freezing (HPF) fixes the sample while preserving the cellular structure in its near-native state.

The following correlative workflow was followed. Single Plane Illumination Microscopy (SPIM) and Spinning Disk Confocal Microscopy (SDCM) were used for visualizing *Autophagy atlas*, which provides cell specific information about the autophagosome creation, dependent on various stress conditions. After a desired condition was imaged, the root is quickly high pressure frozen, to preserve the intercellular activity as it was observed with the advanced LM techniques which enables correlation. To assess the orientation and shrinkage of the root after the fixation protocol, we introduced an intermediate step. Two strategies were followed:

- (1) A commercially available Correlative Light and Electron Microscope (CLEM) was used after the sample had been prepared for TEM, sectioned and placed on the sample grid. Epoxy resin, which samples are usually embedded in for TEM, does not preserve fluorescence. However, this is crucial to re-find the autophagosomes of interest after embedding and assess the quality of sample fixation, therefore, alternative embedding in Lowicryl resin was introduced.

(2) The second strategy was to image the root using Micro-Computed Tomography (μ CT) after resin embedding. As to our knowledge, μ CT 3D reconstructions of root tips have not been published yet. To reduce noise, it was necessary to trim the surrounding resin. Additionally, the root was stained for longer time periods. Lastly, autophagosomes were placed into cellular context using TEM.

It is extremely exciting to be on the forefront of method development when many possibilities are yet to be discovered. We believe there are still many combinations that will help to understand biomedical processes better and it is on us, scientists, to try and work with the modalities available and develop new correlations. This is what this project is all about, correlating known modalities to discover the unknown.

2 Motivation

There is a great need for a useful new method that allows us to visualize autophagy in plants both in-vivo and on the ultrastructural level. Correlating advanced LM and TEM is the most feasible option as studying fluorescent proteins dynamics with advanced LM, is followed with TEM, which provides an intercellular context. Correlative imaging enhances the best features of modalities and uses them to overcome the limitations of imaging within the whole spatial-temporal context. Additionally, correlative imaging of the same region of interest provides a validation of conclusions obtained with one of modalities. Processes can be identified with LM and further explored with EM. In the past years, correlative imaging has been advancing significantly as shown in Graph (1), CLEM often being implemented in biology. There is however a big gap between imaging live samples with one modality and fixed samples with the other, especially when the visualized organisms are relatively large. Specifically, to our knowledge, SPIM and TEM have never been correlated before.

The method was developed to visualize the location of all ATG8 proteins (ATG8 A - ATG8 I) under various stress conditions within living root cells with advanced LM and observe the action in more detail on a cellular level with the help of TEM. SPIM, with its little photo toxicity, high resolution in z and fast volume imaging is an ideal tool for capturing autophagosomes in the living root. Similar results to SPIM are achieved with SDCM, and a comparison between the two approaches was made. Different stress conditions are expected to result in various ATG8 proteins appearing in different parts of the root. An *autophagy atlas* for each of the ATG8s and for each stress would help with deeper understanding of autophagy selectivity in plants. It is still uncertain whether autophagosomes always get created near certain organelles or if it varies based on cell types and how the double membrane is formed. Therefore, providing intracellular information to the atlas brings additional value and validation. The potential of this

method development also lies in its application to many other biological samples in- and ex-vivo.

3 Theoretical Framework

3.1 Confocal Microscopy (CM)

The first confocal microscope was patented in 1957 by Marvin Minsky, which opened the door to 3D imaging. At first 3D acquisition was quite slow but already in the 1960s Mojmir Petran developed the first commercial confocal microscope with improved speed. In the early 1970s, M. Davis Egger and Paul Davivovits first described confocal microscopy (CM) using a laser beam as an illumination source and received a U.S. patent for it. In the mid-1980s, the first commercial fluorescence confocal microscope was introduced and soon the exquisite and convincing capabilities of CM were shown to the world's biological community by J.G.White, W.B. Amos and M. Fordham [3]. Ever since then, CM has been an indispensable imaging technique in biology and material science. [4]

Although conventional wide field optical systems are useful tools, they cannot be used to scan thick samples. This is because they do not discriminate between in-focus and out-of-focus light, collecting all the scattered light of the excitation area as can be seen on the Figure 1, which results in a reduced quality of the image. CM overcomes this by using a laser excitation source which provides high-power point illumination. The sample is scanned line by line with a focused laser beam. By using a pinhole aperture, placed right in front of the detector in the conjugated plane, only the emitted fluorescence from the plane of interest reaches the detector. [5]

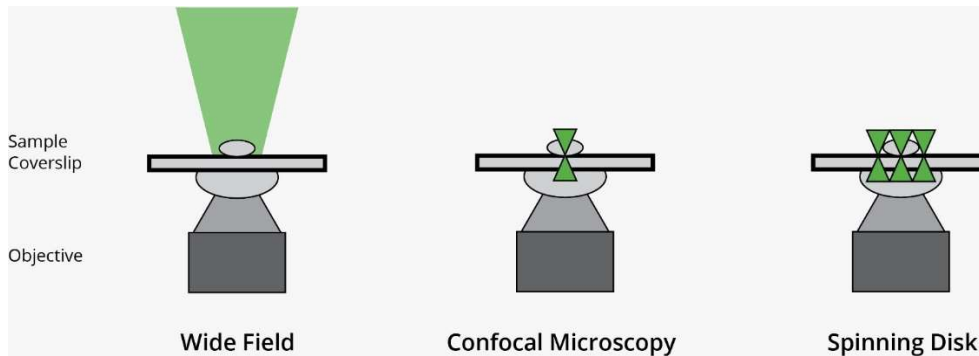


Figure 1 Even though wide field microscopy is useful, scanning thick samples is not feasible. CM with its point illumination and pinhole overcomes this problem, but requires a lot of time to scan through thicker samples, which is fine for fixed samples, but for live samples, spinning disk might be a better option, as it reduces scanning time with adding multiple pinholes to the system. Figure adapted from [6].

3.1.1 Principles of CM

CM reduces the collection of out-of-focus light using a pinhole. A laser light beam is focused onto a fluorescent specimen through the objective lens. The mixture of reflected and emitted light is captured by the same objective and is directed to a dichroic mirror. Reflected light is deviated by the mirror while emitted fluorescent light passes through. The confocal aperture reduces out-of-focus light. Focused light then passes through an emission filter and proceeds to a photomultiplier. [7]

Confocal microscopes illuminate points that can be as small as $0.25\mu\text{m}$ in diameter and $0.5\mu\text{m}$ in depth in z-direction. This depends on the design of the microscope, wavelength of incident light, objective lens, settings of the system and the specifications of the specimen. The point only illuminates the sample at one specific spot at a time and is moved along the sample until scanning the entire plane of interest. The unique design of the microscope allows to detect only in-focus excitations of the specimen. It also improves the spatial resolution and contrast. The name confocal stems from the arrangement of the illumination source, specimen and detector being in the sample plane of focus [5].

Airy disk

The bright spot surrounded by darker rings is created by diffraction of light passing through the lens system and is called Airy disk. The best image quality is achieved when the pinhole is set to the size of the Airy disk to eliminate resolution-limiting aberrations. This however, reduces the overall brightness of the image which can be a hindrance when dealing with an already low signal. Although increasing the aperture will help with the brightness, it will negatively impact the axial resolution. [5]

Spatial resolution

When using microscopy to image samples, spatial resolution and temporal resolution are of importance. Spatial resolution can be divided into lateral spatial resolution, which gives us information about the resolution along the x - and y -axis, and the axial spatial resolution corresponding to the resolution along the z -axis. The lateral spatial resolution determines the minimum resolvable distance d between two points in the horizontal x, y -plane of the confocal microscope. When trying to produce an acceptable contrast in the CM, the separation of points required to do so is reduced because of a narrower intensity point spread function. In the following we give an equation for this reduced distance:

$$d_{xy} = \frac{0.4 \lambda}{NA} \quad (3)$$

Resolution along the z -axis is described below, where n is the refractive index of the material:

$$d_z = \frac{1.4 \lambda n}{NA^2} \quad (4)$$

The lateral spatial resolution in CM is 2-3 times better than the axial spatial resolution in the same imaging conditions with a non-confocal setup. [5]

Temporal resolution

Temporal resolution is determined based on the scan speed and the quality of the detector. Its speed of converting the analogue information to digital and therefore its processing rates influences the temporal resolution greatly. Computers capability can improve temporal resolution as well: 1-2 frames per second (fps) for a 512×512 pixel image is a typical speed, but rates of 100 fps or higher can be recorded when images are smaller [5].

Dynamic range

Resolution of light intensity is described by the dynamic range. It is defined by a number of grey values in the image when it is converted from an analogue to digital signal. It can also be described as the ratio of saturated signal (largest signal) to noise (lowest signal). The dynamic range is given in Volts or number of electrons. By adjusting electronic gain and offset, the amplitude range is modified. The values should be set such to fill the entire dynamic range, starting from black (no signal) to a white or saturating signal. This will come closest to the full imaging potential of the detector [5].

Signal to noise ratio

Another important imaging condition is the signal-to-noise ratio which influences the visibility and clarity of the image. The signal-to-noise ratio is affected by the background, the thickness of the specimen and the noise of electronic components included in the built microscope. If an image is bright, the main contributors to the signal noise will be the intensities of object and its background. If the image is dim, the electronic noise from the microscope will have a higher influence on the quality. The brightness depends on many factors such as the laser power, fluorophore density in the sample, digital gain, and numerical aperture. A small signal-to-noise ratio results in worse image quality, it can however be improved by increasing the laser power, slower acquisition, pinhole size and by averaging the individual frames. [5]

3.1.2 Spinning disk confocal microscopy (SDCM)

The biggest disadvantage of most confocal laser scanning microscopes is the time required to acquire a single-plane image during 3D image acquisition. The laser illuminates only a single point at a time, which is time consuming, therefore a trade-off between the image resolution and acquisition speed must be made. SDCM overcomes the problem of acquisition speed with the help of the multiplex principle. The scanning unit has two coaxially aligned disks (Figure 2) with spirals consisting of thousands of pinholes and a dichromatic mirror in between. As the disk spins, every 30 degrees an image is produced which makes it possible to acquire up to 2000 frames per second by regulating the speed of disk rotations, allowing multipoint scanning. [5]

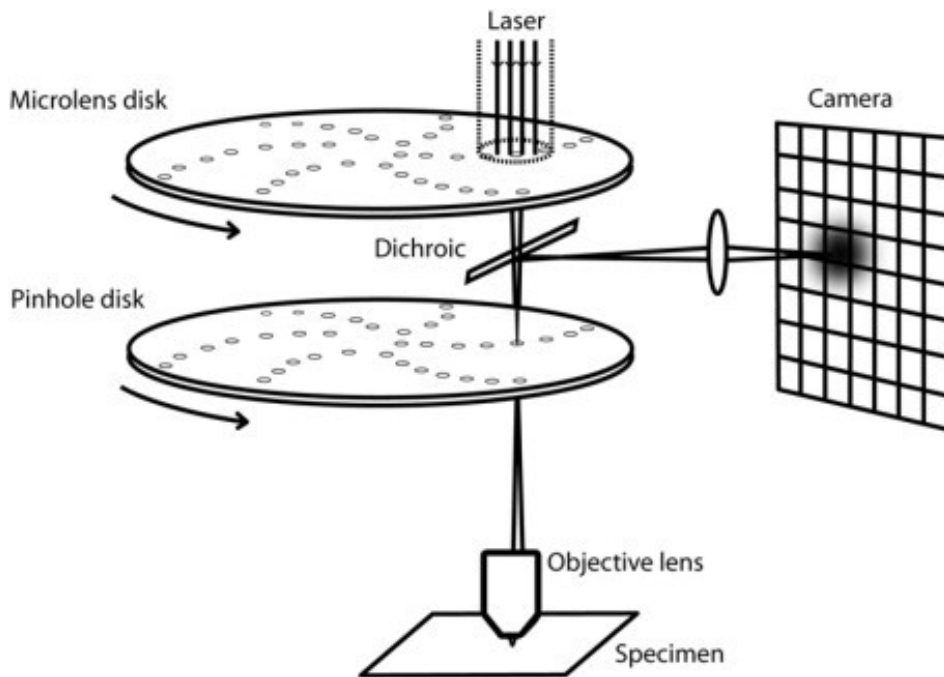


Figure 2 Spinning disk setup. Much faster scans can be achieved due to multipoint scanning. With its two disks, up to 2000 frames can be acquired per second. Figure is taken from [8].

3.2 Light Sheet microscopy (SPIM)

Light sheet microscopy or SPIM allows selective plane illumination and is the method of choice when it comes to scanning big, sensitive

samples for a long period of time. SPIM's high-speed, full-frame image acquisition, alongside with its reduced photo toxicity and an option for multi-view sample rotations makes it a powerful technique for long-term whole-volume observations. Even though the idea of using light sheets as a sectioning tool in a sample has been around since the first publication by Siedentopf and Zsigmondy in 1902 [9] that describes a very simple version of SPIM, first applications of SPIM in life sciences were seen only relatively recently. Ever since it was introduced in 2004 [10], SPIM has proven to be very useful for a variety of applications, especially for biological samples that are large and sensitive. A good example are plant roots or drosophila and zebrafish embryos that can be up to a few millimetres in size. Conventional microscopes cannot image thicker samples without sectioning techniques, due to limitations in penetration depth and acquisition time. SPIM has overcome that challenge with multi-view sample rotation and single-plane illuminations. Additionally, SPIM solves the issue of photo toxicity with limiting illumination of the sample to only a slice at the time. It is now possible to observe cellular and morphogenetic events in real-time in the entire sample of up to several mm for time periods of several days (*in-toto* imaging).

Evidently, SPIM also has its own limitations: One of the biggest is the fact that the sample needs to be transparent - which requires sophisticated clearing techniques. The large volume of the image data set complicates handling the acquired images. [11]

3.2.1 Principles of SPIM

Unlike usual single-lens setups, SPIM uses two optical paths. Wide field detection is perpendicular to a thin light sheet illumination positioned exactly in the centre of the field of view. The detection objective collects light, passing it through the fluorescence filter to the tube lens which then projects the light onto the detector. This is illustrated in Figure 3. There is no need for a dichroic mirror in the detection path as the light source is perpendicular to it.

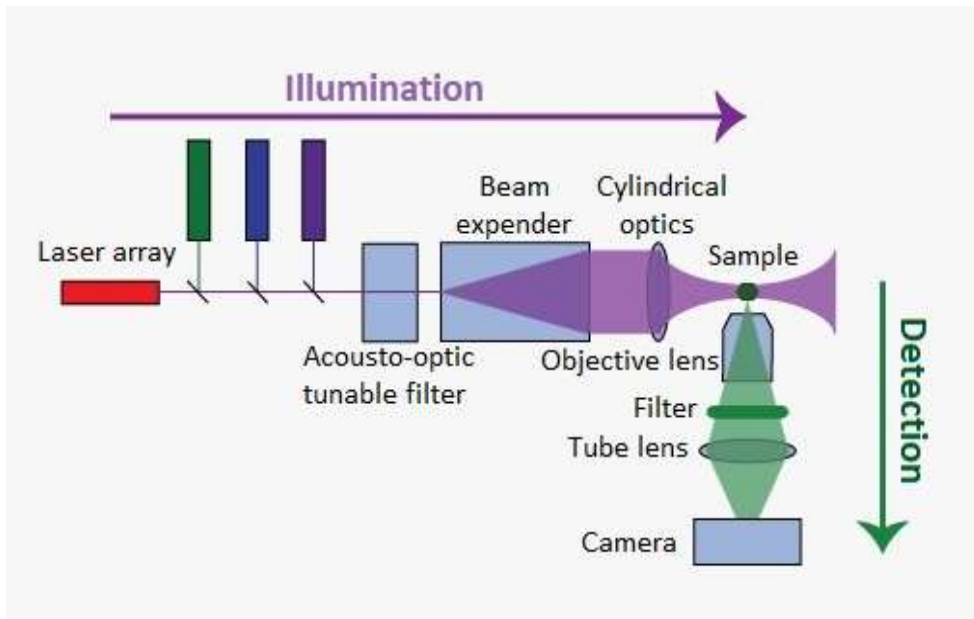


Figure 3 SPIM illumination and detection paths are uniquely positioned perpendicular. With its sheet of light, SPIM illuminates a whole slice of the sample at once and therefore increases speed and minimized phototoxicity. Adapted from [11].

The excitation path starts with the coherent light source and includes the optics necessary to create the light sheet: There are two ways to create a light sheet and therefore two different light-sheet microscopy setups. Cylindrical optics are simple to implement and do not require moving elements. Cylindrical lens illuminates the entire field of view at once and hence uses little power per line and has a quick acquisition time. Another way to create a light sheet is with rapidly scanning beam up and down. This set up is slightly slower in the acquisition time, however its light sheet's intensity is more homogenous and easier to adapt. Special techniques are available for this set up, e.g. production of a Bessel beam or two-photon excitation. By changing the amplitude of the beam, it is possible to alter the height of the light sheet and by adapting the diameter of the beam, different thicknesses can be set.

Some of the most important properties of a light sheet are the thickness, uniformity and its penetration depth. Based on the sample,

the light sheet can be very thin (approximately 1 μm) or thicker (approximately 6 μm). With this optical arrangement, SPIM solves the fundamental issues of single-lensed system, such as phototoxicity and obtaining thin optical sections at low numerical aperture objectives. It also reduces acquisition time since it illuminates the entire plane of interest instead of a point as done for CM. The detector collects photons simultaneously for the entire illuminated plane during the entire exposure time - without the need to scan the sample point by point. Because of this efficient parallel recording the exposure time can be drastically reduced. SPIM offers an excellent signal-to-noise ratio and minimal photobleaching considering the fast and sensitive data acquisition. It is also useful when it comes to larger samples as it operates well even with a low numerical aperture, low magnification and short working distance. Light sheet microscopes are usually built according to the sample and the biological question, therefore horizontal and vertical arrangements are common. Some have the additional feature of a rotational stage [12].

3.3 Micro-computed tomography (μCT)

The commonly known imaging technique called Computed Tomography (CT) is a non-invasive and non-destructive 3D imaging modality that can visualize bone and - after treatment with contrast agents - inner organs with good contrast. μCT is an advancement based on the same physical principles as clinical CT. However, it enables us to image significantly smaller samples with high resolution and provides detailed anatomic information. It does not require any sample sectioning or histological slicing. In the early 1980s, the application of the CT technology was extended from clinics to the research field. In research, higher resolution and longer exposure time were not an issue as it is in clinical CT, where it is necessary to be aware of patients' safety. The first X-ray microtomography system was conceived and built by Jim Elliott in the early 1980s [13]. Feldkamp was the first to build a micro-CT scanner for analysing trabecular bone structure not

visible with CT [14]. It already became commercially available in 1994 and soon became an irreplaceable and essential imaging tool for bone research, quantifying structure-function relationships, disease progression, and regeneration in preclinical models. In the last few years, the availability of μ CTs has grown and its applications in biomedical research have increased.

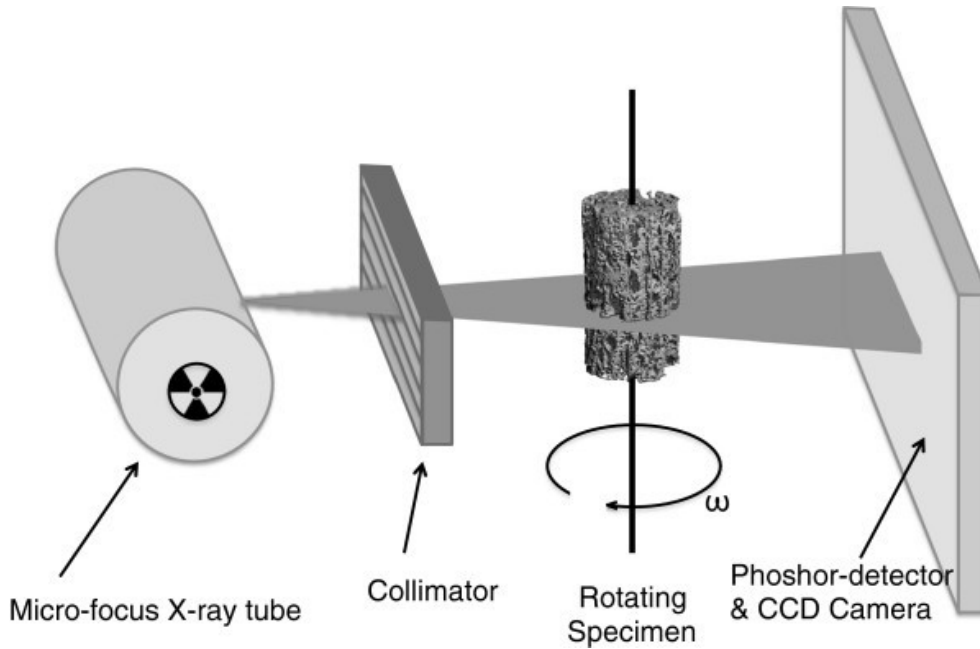


Figure 4 Components and a setup of μ CT. Unlike in clinical CT, in this setup the sample is being rotated in order to acquire a 3D image. Figure is taken from [15].

3.3.1 Principles of μ CT

Micro-computed tomography is a valuable imaging tool that produces high resolution 3D images out of 2D trans-axial projections or slices of a sample. μ CT consists of several major components: An X-ray tube, a radiation filter and a collimator which focuses the beam geometry to either a fan- or cone-beam projection and which is placed in front of the sample. Specimens are fixated on the stand, positioned in front of a charge-coupled device camera. The setup is shown in Figure 4. The fan-beam system is based on a one-dimensional X-ray detector and an electronic X-ray source, creating 2D cross-sections of an object. The cone-beam system is slightly different as it is based on

a 2D X-ray detector and an electronic X-ray source, which creates projection images that will later be used for the 3D reconstruction. Acquisition of a 3D volume is performed by rotating either the sample or the emitter and detector to generate a series of 2D projections. These will then be transformed into a 3D representation using back projection. Micro-CT's non-destructivity and its high resolution with a voxel size of only 1 μm makes this technique a very valuable asset with being non-invasive and precision. [15]

Micro-CT's signal is based on the attenuated intensity of X-rays passing through the sample. The intensity of X-ray beam is reduced as it passes through tissue. This happens according to the equation

$$I_x = I_0 e^{-\mu x} \quad (5)$$

where I_0 is the intensity of the incident beam, x the distance from the source, I_x the intensity of the beam at distance x from the source, and μ is the linear attenuation coefficient. Linear attenuation coefficient describes the fraction of attenuated incident photons in a monoenergetic beam per thickness of a material. The intensity of the beam on the other side of the sample depends on the material of the sample and the source of energy. Based on the attenuated intensity at the detector, the density of the object can be assessed. [15]

3.4 Transmission Electron Microscopy (TEM)

TEM was first developed because the resolution of LM techniques were limited by the wavelength of visible light. In 1925, Louis de Broglie started to theorize about electrons having wave-like characteristics. In 1932, a paper was published by Knoll and Ruska describing the first EM [16]. To emphasize the importance of this discovery, first commercial TEMs were developed only 4 years after this breakthrough. A huge motivation for scientists was the fact that accelerated electrons have a smaller wavelength than visible light photons. By increasing the energy of the electrons to approximately

100keV, the wavelength corresponds to a few picometres. To compare electron microscopy with LM we can use this equation that demonstrates the relationship between the resolution and the electron wavelength:

$$\delta = \frac{1.22 \lambda}{\beta} \quad (6)$$

where λ is the electron wavelength and β the semi angle that electromagnetic lenses collect, which is same as Equation (1), as wave-like electrons have the same resolution-wavelength relationship as photons. Electromagnetic lenses are not as refined as glass lenses used in optical LM. Aberration-correction in lenses is limited and costly. This means that, despite of electron wavelengths of only a few pm, the EM used for biological soft-tissue samples cannot achieve a resolution below atomic level [17]. However, recent developments in cryo-EM have allowed biological structures as small as 2 Å to be resolved [18].

3.4.1 Principles of TEM

The way an image is formed in an EM does not greatly differ from the phase contrast LM. Instead of light and glass lenses, electron microscopy uses an electron beam that is collected by electromagnetic lenses. To prevent electron scattering by air, a high-level vacuum is needed in the microscope. This is achieved by a vacuum in the microscope during the entire acquisition process. The sample must be completely dry. The electron beam is emitted from an electron source, also called electron gun. After emission, the electrons are accelerated using a high potential of several hundred kilovolts. There are two types of guns available, the field emission gun and the thermionic electron gun. The latter uses a heated filament (cathode), usually made of Tungsten or Lanthanum Hexaboride. The path of rays can be seen in Figure 5. Electrons are extracted and accelerated through a Wehnelt cylinder. A Wehnelt cylinder is a biased grid that has a potential

hundreds of volts different from the filament, which results in the cross-over of electrons. The size of the electron beam at the cross-over can reach down to few tens of a micron. The generated beam then travels down through the column. Before imaging a sample, the beam is aligned to assure optimal illumination. The alignments are done with electromagnetic lenses that use magnetic fields to influence the electron path. The condenser system consists of two or more lenses and an aperture. It adjusts the convergence or parallelism of the beam with a controlled spot size. The first condenser lens makes an image from the beam at the cross-over and the second condenser lens changes the beam size. The condenser aperture controls the size of the beam that proceeds down the column and therefore the intensity of the illumination. The beam travels through the upper objective lens, which is right above the specimen chamber, then through the ultra-thin sample where parts of the electrons are diffracted. The objective aperture stops electrons diffracted at a large angle from continuing their path towards the detector. This improves contrast and reduces noise. The lower objective lens collimates the diffracted and non-diffracted waves and focuses them. The intermediate lens will magnify the initial image from the objective lens and passes it on to the projector lenses, which will magnify it according to the selected magnification. Not all projector lenses are always needed for lower magnifications. The image is then projected on the image plane. The electrons are either converted to photons using a charge-coupled device

before being recorded by a camera or detected using a direct electron detector [19].

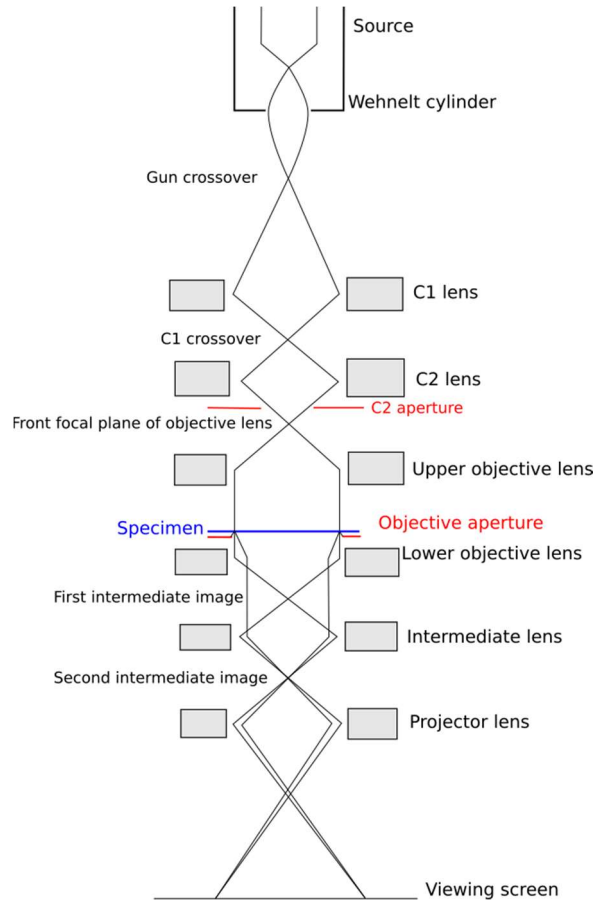


Figure 5 Ray diagram in EM. Electrons travel from an electron gun through a series of lenses and the ultrathin sample to the detector. Image taken from [20].

Biggest limitation in TEM is the sample itself as it is composed of light elements. Using phase contrast, this does not give much contrast at all, specifically for cryo-TEM. Chemical fixation and staining alleviate the limitations, but at the cost of ultrastructural changes in the specimen. Spherical aberrations are also a difficulty, which broaden the point spread function and reduce resolution significantly. This results in blurriness and delocalization. Spherical aberration correction is being implanted in some microscopes nowadays. Correcting spherical aberration leaves us with correction of the effects of chromatic aberration as the next major issue and possibility to improve TEM.

Chromatic aberration corrections are more complex in some cases, but have already been incorporated into some newer microscopes. [21]

3.5 Correlative Light and Electron Microscopy (CLEM)

Correlative microscopy uses two or more imaging modalities to image the same sample. With this approach, which is also described in Figure 6, we are able to gather additional and complementary information. Correlative microscopy was first used for the correlation of LM and EM, which is still the most used correlative microscopy method. The correlation of LM and EM is called correlative light and electron microscopy (CLEM).

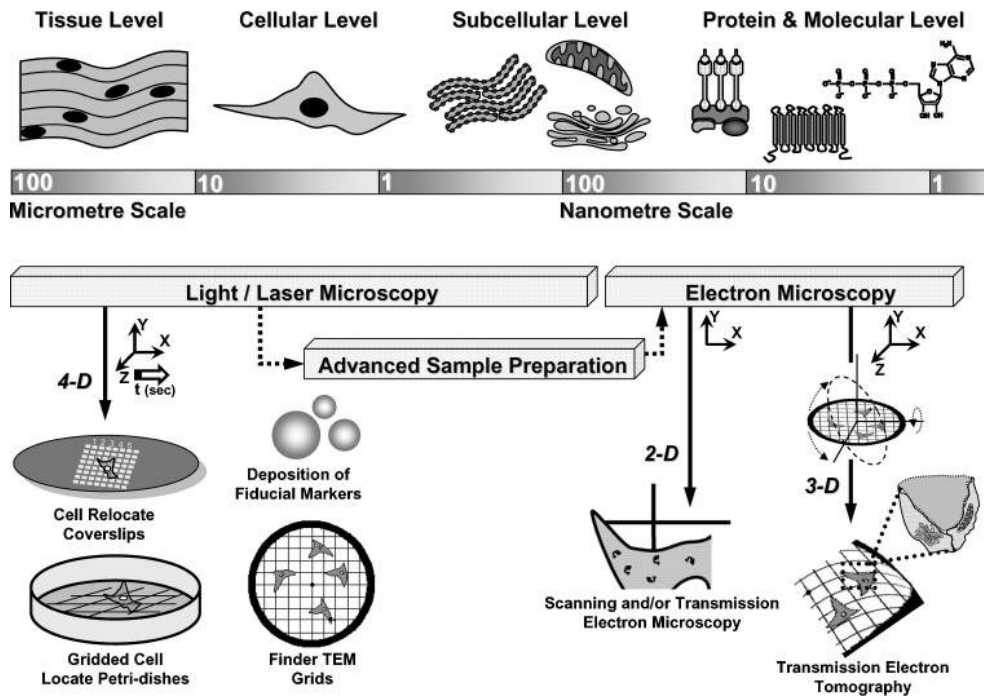


Figure 6 The integration of LM in EM. With CLEM, the temporal and spatial resolution gap is overcome. As seen, there are many approaches of CLEM. However, most used protocols investigate the sample already on the grid. Figure is taken from [22].

The aim of CLEM is to bridge the gap between spatial and temporal resolution. LM allows for rapid scans of larger areas. Electron-mediated EM can achieve high magnification and better resolution. The combination of both methods allows to locate and observe fluorescently

labelled areas of interest and then further investigate the ultrastructure at the exact same location in the EM. The term correlative microscopy was first used in the 1970s when first attempts were done towards establishing a correlation between the two methods, but it was not until later, in the second half of the 1980s, that scientists began implementing the technique for biological samples. At first, CLEM was done in a rather crude manner, not using fiducial markers to help relocate the sample with other techniques after changing imaging platforms. Microtome scratches or latex depositions were used. Currently, there are several labelling techniques and markers commercially available [22], including genetically encoded probes for pre-embedding labelling, metal tagging, non-genetically encoded probes for pre-embedding labelling and post-embedding labelling for fluorescence in EM sections. [23]

As there are many LM and EM techniques, there are quite a few variations of CLEM. Broadly speaking, there are two main CLEM options, Correlative Fluorescence Scanning Electron Microscopy (CFSEM) and Correlative Fluorescence Transmission Electron Microscopy (CFTEM). The name suggests that the methods differ based on the EM approaches. Scanning electron microscopy (SEM) gathers topological information while TEM presents data from a thin cross-section of the sample. CLEM can be classified based on its sample preparation and fixation or based on the size and permeability of the sample [22]. Classical TEM sample preparation, such as chemical fixation and plastic embedding, destroys fluorescent labelling. Chemical fixation protocols can be adapted to preserve fluorescence, but this is at the expense of ultrastructural preservation. An alternative to chemical fixation is cryo-fixation, which avoids fluorescence reduction due to acidic and oxidizing environment created by Osmium tetroxide and UA and does not require complete dehydration. Cryo-fixated samples are preserved as close as possible to their native state. CLEM can be performed with LM while the sample is not yet fixated and followed by fixation for EM analysis. In this case EM fixation does not need to be altered. In the case where the sample is already fixated and

placed on the grid prior to both LM and EM, alterations to the protocol are needed. The latter option allows analysis with available integrated microscopes that recently became available. [23]

3.6 Near-Native Sample Fixation

3.6.1 High Pressure Freezing (HPF)

The vacuum in the TEM requires samples to be absolutely dry. Due to the nature of the interactions between electrons and matter, the visualized section must be ultrathin. To achieve the necessary thinness and dryness in biological samples, they need to be prepared with a number of invasive steps. For bigger samples like roots, one of the most widely used techniques is chemical fixation, where samples are fixated by various chemicals and water is replaced by an organic solvent (like acetone, methanol, ethanol, ..) to allow for better infiltration of resin.

Most commonly aldehydes are used for fixation as they cross-link proteins. To assist with lipid stabilization, osmium tetroxide (OsO_4) can also be added. However, fixation is not uniform and it creates a gradient during the penetration of the tissue which leads to the fixation of outer parts of the volume while the inner parts remain unfixated. The following steps are dehydration and embedding. Dehydration is necessary as resins are usually hydrophobic and in order to allow for proper infiltration of the resin into the sample, water needs to be completely removed. This is usually done with the organic solvents acetone or ethanol. As chemical fixation consists of many steps, it is hard to assign the deformations of some samples to a specific step, however it is known that lipids are often extracted, and protein loss also occurs. Additionally, not all compounds of an organism can be fixated and preserved with chemical fixation. This is why other fixation techniques were developed [24].

A fixation alternative is rapid freezing of the sample to arrest all cellular processes at the same time. One of the main components of a biological sample is water, therefore understanding the behaviour of water helps to understand the freezing of samples. Water molecules

consist of an oxygen atom and two hydrogen molecules connected by a covalent bond each. Water molecules interact with each other via hydrogen bonds. Based on the state water is in, hydrogen bonds behave differently, as can be observed in Figure 7. When water evaporates, hydrogen bonds are broken. In liquid state, hydrogen bonds are present but can be broken and bent. When frozen, molecules form four hydrogen bonds with each other and therefore a crystalline array. Based on the temperature and pressure, freezing will result in either hexagonal ice, if frozen at a slow cooling rate, or in cubic ice, if frozen rapidly. If the cooling rate is further increased, the nucleation event is avoided and ice crystals do not form. This is the ideal condition for preserving the structure within the sample and avoid diffraction spots while imaging. [25]

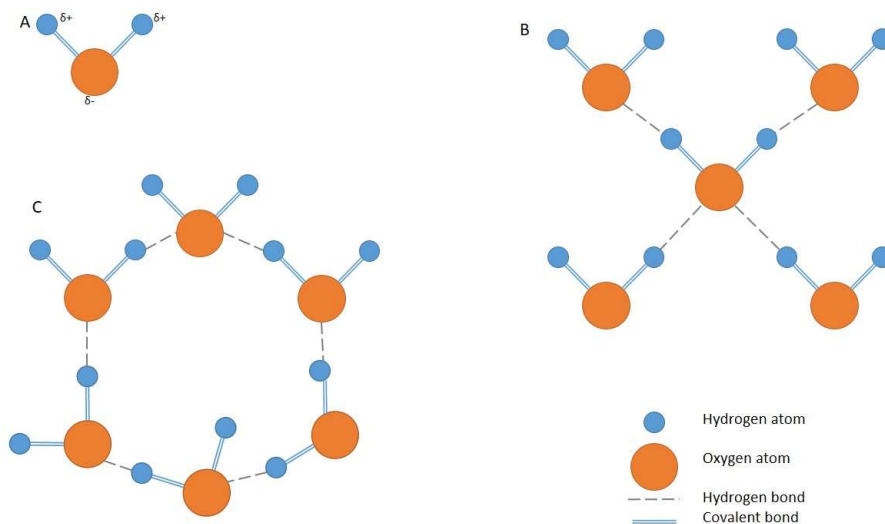


Figure 7 Three states of water. *A* represents water as a gas, when no hydrogen bonds are being formed. In *B*, water is in its liquid state. A water molecule binds to a maximum of four other molecules and is then at the centre of a tetrahedron. Hydrogen bonds are being created but are also easily broken. *C* represents hexagonal ice.

Rapid freezing fixates and stabilises biological materials as a preparation for electron and cryo-electron microscopy. In recent years, cryo-preparation and cryo-electron microscopy have been widely used

because they produce fewer artefacts during preparation in comparison to chemical fixation and room temperature processing. There are two distinct advantages of cryo-fixation over chemical fixation. Firstly it is achieved within milliseconds and secondly it ensures simultaneous immobilization of all macromolecular components and causes less ultrastructural deformations. Many protein networks are very labile and fall apart with changes in osmotic conditions or temperature. During cryo-fixation these unwanted effects are minimized. Besides plunge- and slam-freezing, HPF is extremely useful as it is able to modify the freezing behaviour of water to enable freezing of larger samples up to 200 μm . It was first developed by Moor and his colleagues in 1968 [26]. This non-invasive method is based on the conclusion that the nucleation of ice crystals is both temperature and pressure dependent. The transformation of water from the liquid to the crystalline state is accompanied by an increase in volume which is prevented by the application of high pressure.

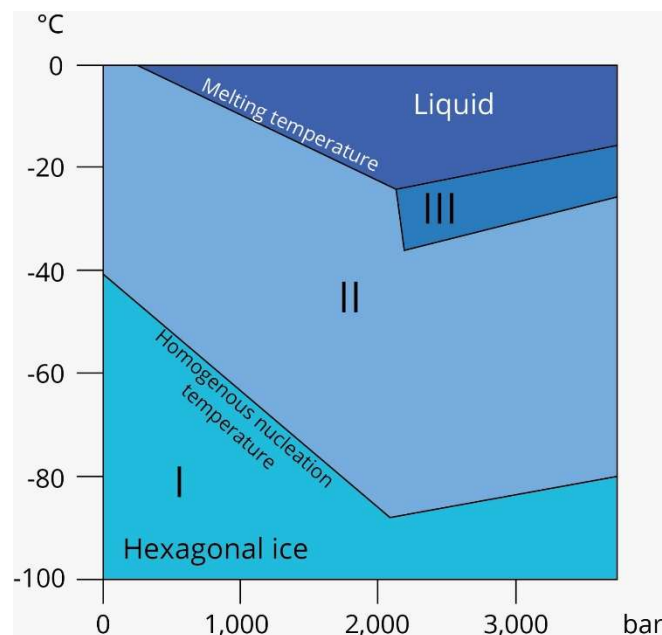


Figure 8 Characteristics of water under various pressure, I, II and III being different forms of ice. We can observe that the melting point at 2100 Bar falls to -22°C. In order to achieve nucleation of the ice, only -92°C is needed which is what high-pressure freezers can achieve. Image adapted from [27].

The melting point of water and the temperature for the nucleation of an ice crystal in pure water are lowered to -22°C and -92°C under a pressure of 2100 bar as shown in Figure 8. Therefore, lower cooling rates are required to vitrify samples compared with freezing at ambient pressure. Currently high-pressure freezing is the only method to vitrify thicker samples of up to 600 μm . Rapid freezing can arrest the biological processes of a sample, as long as it remains frozen. There are two options after HPF, the sample can either be sectioned while frozen under cryo-conditions and imaged with cryo-EM or be dehydrated, embedded in resin, sectioned and imaged with TEM. The latter requires a procedure called freeze substitution. [24]

3.6.2 Freeze substitution (FS)

Freeze substitution (FS), a method that dissolves frozen water at low temperatures, was first described in [28]. In Fernandez-Moran's work, FS was first modified to make it feasible for EM. With these modifications structural preservation was improved. One of the suggestions for improved preservation was embedding at low temperatures [29]. The results of this gave motivation to other research groups, which over the years adapted and optimized protocols to overcome the poor penetration of heavy metals and difficulties with the visualization of cell membranes.

The ideal FS medium remains fluid at -85°C , when water in biological samples recrystallizes. The medium also dissolves water within the time limits and presents low risk to humans. The solvents that have been used in the past are acetone, methanol, ethanol, heptane and diethyl ether, with acetone and methanol being the most commonly used. Extraction of carbohydrates, proteins and lipids remain a problem. After Humbel demonstrated the benefit of adding 0.5% UA to methanol, other fixatives started to be added to FS mediums [30]. When choosing an appropriate fixative, multiple things should be considered as various fixatives contribute to different

preservations. Fixatives that can be added are osmium tetroxide, uranyl acetate (UA), acrolein, glutaraldehyde or formaldehyde and tannic acid. Osmium tetroxide preserves unsaturated lipids especially well. Glutaraldehyde surpassingly crosslinks proteins and UA contributes to the stability of the cell's structure [30]. In order to enhance membrane contrast, contrast agents can be added, however adding 1 to 5 % water has also proven to be reliable. [25]

3.7 Biological Background

3.7.1 Autophagy

Even though there are many differences between eukaryotic cells across the kingdoms, they share main characteristics that differentiate them from prokaryotic cells. One of those characteristics is autophagy. During the lifetime of a cell, components passing through the cell have potentially toxic effects. These components (cargo) include aged proteins, damaged organelles, malfunctioning ribosomes, or protein aggregates. Autophagy, meaning self-eating, is the natural process in eukaryotic cells responsible for recycling and degrading unnecessary or dysfunctional cellular components. Autophagy plays an important role in cell survival and maintenance as it is a vital adaptive response to stress. It operates by selecting unwanted components in the cell and surrounding them with a double membrane vesicle created specifically for this purpose [31]. There are four types of autophagy: Chaperone-mediated autophagy, microautophagy, macroautophagy and mega-autophagy. It was shown that dysfunctionality of autophagy is strongly connected to many diseases, for instance cancer [31], [32], thus motivating extensive research in the past few years aimed at a better understanding of this process present in all of our cells.

Chaperone-mediated autophagy

So far only found in mammalian cells, it does not assimilate the unwanted components within the cell with the help of a double membrane but directly identifies the cargo protein which is then

unfolded and immediately translocated to the membrane of lytic organelles. Chaperone-mediated autophagy targets the protein that contains the KFERQ consensus motif which is then unfolded and relocated to the lysosomes' membrane where it is recycled into the lumen. This kind of autophagy can degrade many proteins, calcium, lipid-binding protein, vesicular-trafficking protein and certain glycolic enzymes. [33]

Microautophagy

This is a process where the cytoplasmic content is processed inside the lytic organelle of the cell by invagination (folding itself in) and deformation of its membrane. Microautophagy occurs directly on the membrane and can affect intact organelles as well. [33]

Macroautophagy

It is the most researched of the four types and, unlike the other two, it happens outside of the lytic organelle. The origin of the double membrane is not completely certain. The double-membrane vesicle that is created is called an autophagosome. Its role is to capture the cargo and bring it to the lysosome or vacuole for degradation. [34]

Mega-autophagy

Mega-autophagy massively degrades the cell and most of the time brings it to a programmed cell death. It permeabilizes or raptures the vacuole membrane, leading to a release of hydrolases into the cytoplasm. This results in total degradation and therefore apoptosis. [35]

While they are all different in their structure and role, all types of autophagy identify the cargo and degrade it with the help of the lytic compartment of the cell. Although it was assumed that autophagy is unselective, it is now known that autophagy operates selectively, meaning that various cargo is recognized and assigned to the

enveloping autophagic membrane. That way certain components in the cells can be eliminated only when needed. [36]

3.7.2 Autophagy in *Arabidopsis* roots

We can find several mechanisms for the recycling of intercellular constituents in plants: One of them is autophagy. Mechanisms of autophagy in plants have been closely studied in the last couple of years and with new discoveries, the selectivity of the autophagy and the importance of dedicated receptors have now become of great interest. Autophagy occurs relatively rarely yet persistently in plants. It is indispensable during changes of the environment and other stress periods, as it is crucial for the plant's metabolism, energy balance and allocation of the nutrients within the organism.

So far, only microautophagy, macroautophagy and mega-autophagy have been observed in plants (Marshall & Vierstra, 2018). Microautophagy and macroautophagy are illustrated in Figure 9.

As described before, microautophagy gathers the cytoplasmic material that need to be degraded to the vacuole and, with folding the vacuole's tonoplast, traps the material inside where it is then recycled. Macroautophagy captures the cargo by creating a vesicle called autophagosome and mega-autophagy degrades the entire cell. To this day, we are still missing much information about the underlying mechanism of autophagosome formation in plants. In some cases, the double membrane is created at the endoplasmic reticulum, in others it forms itself from tubular formations that coalesce into a cage-like form.

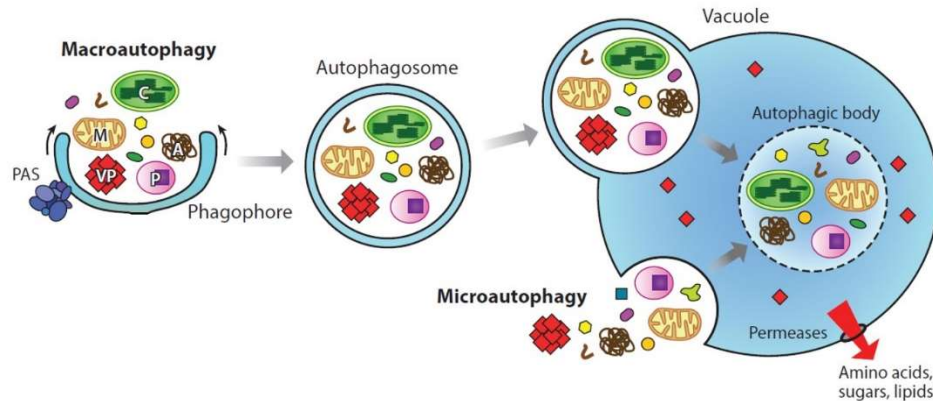


Figure 9 Macroautophagy and microautophagy in plants. At first, phagophores are created, surrounding the components of the cell that need to be digested. In microautophagy, the components are folded into the vacuole. Figure taken from [35].

Autophagy in plants is mediated by the many autophagy-related proteins, called ATGs. They send signals with information about the stress levels in the cell to the lipids and regulatory proteins. Those then trigger the pathway to the vacuole for the autophagosome. 40 ATG proteins have been connected to selective and/or non-selective autophagy, responding to various cell states. Autophagy is strongly induced when the cell is exposed to stress.

Most of what we know is based on the characterization of these ATG protein complexes and their role in autophagy. ATG proteins are responsible for a large number of processes in the autophagy machinery. Disruption of one of the genes encoded for an ATG protein results in a hypersensitive plant. ATG proteins have various roles: ATG1 is responsible for the initiation of the bulk autophagy in yeast, for example; ATG9 is the only conserved integral membrane protein in the pathway, and ATG2 and ATG18 target the autophagic membrane. Even though they are essential, their biochemical functions are not yet well understood. [35]

Among the proteins involved in the autophagy machinery, ATG8s are the ones studied the most and of interest to us. They are helpful proteins for studying the core autophagy machinery as they are linked to the lipid phosphatidylethanolamine and serve in lipidation of the phagophore. The phagophore membrane is expanded until it is fully closed into a circle and then forms an autophagosome. ATG8s can be found both on the autophagosome and autophagic bodies and are therefore a widely used protein for visualization of autophagosomes. There are nine ATG8s (ATG8 A – ATG8 I) in plants, many more than in yeast or human cells. It therefore seems they play a more important role in selective autophagy in plants than in other organisms. The reason for the method development was to be able to visualize the location of different ATG8s under various stress conditions within the living root cells and observe the action in more detail on the cellular level with the help of transmission electron microscopy. [36]

4 Materials and Methods

4.1 Correlative workflow

Research in cell biology of plants is largely driven by GFP technologies, therefore we used a transgenic line that expresses a GFP-targeted ATG8-A protein to develop our workflow. ATG8-A GFP-labelled *Arabidopsis thaliana* surface sterilized seeds were germinated on Murashige and Skoog (MS) medium and 1/2 sucrose concentration buffered with 2-(N- morpholino) ethane sulfonic acid (1/2MS + MES) either on a plate or in a gel block. The seeds were fully grown in the growth chamber with 16h daylight cycle, 21°C and 60% humidity. The root tips were then imaged with either SDCM or SPIM to obtain information about the location of the autophagosomes within the living root *in-vivo*. After acquisition of the desired image, the root was quickly moved into a sample carrier filled with a 10 % bovine serum albumin (BSA) solution in phosphate buffered saline (PBS) and was high-pressure frozen. Two embedding materials were used: Lowicryl HM20 resin was used to preserve fluorescence. Fluorescence preservation is necessary to be able to observe the autophagosomes in the ultrathin sections under CM, allowing to re-identify and correlate areas of interest after relocation. Epoxy resin was used to observe the root with μ CT to evaluate the shrinkage and orientation of the root after freezing and embedding. Subsequently, the embedded root was sectioned into ultrathin sections, placed on a grid and observed in the TEM to locate the observed autophagosomes within the cell. The workflow is summarized in Figure 10.

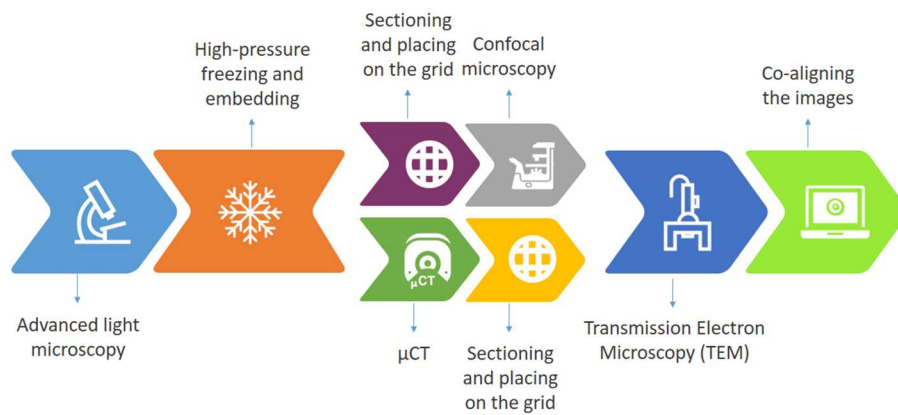


Figure 10 Correlative workflow. It starts with advanced LM and is quickly followed by HPF. There are two options how the workflow can proceed. Either using CM, in which case the samples are embedded in HM20, or using μ CT with the samples embedded in Epoxy resin and stained. After the intermediate steps, TEM assists with visualization of ultrastructure.

4.1.1 Light microscopy and sample preparation

The first step in correlation was to image the sample with advanced LM techniques. We performed CM using an inverted point laser scanning confocal microscope (SPIM780 Carl Zeiss MicroImaging GmbH, Jena, Germany). It is a complete spectral system allowing free choice of detection and the acquisition of lambda-stacks as well as subsequent unmixing for the separation of dyes with overlapping emission spectra. Spinning disk images were acquired with a VisiScope Spinning disk confocal microscope (Visitron Systems GmbH, Puching, Germany), based on a Nikon Eclipse Ti E inverted microscope, equipped with a Yokogawa W1 spinning disc allowing fast confocal acquisition. All components are controlled by the Visiview software. Visiview is Python-based and is fully scriptable. A z-stack of GFP signal was acquired with both techniques.

Sterilized seeds were placed on medium plates like the one in Figure 11 under a sterile hood and sealed airtight. They were moved to the growth chamber for approximately 5 days. Individual roots were then

placed on the glass slide with a droplet of water and covered with a cover slip.

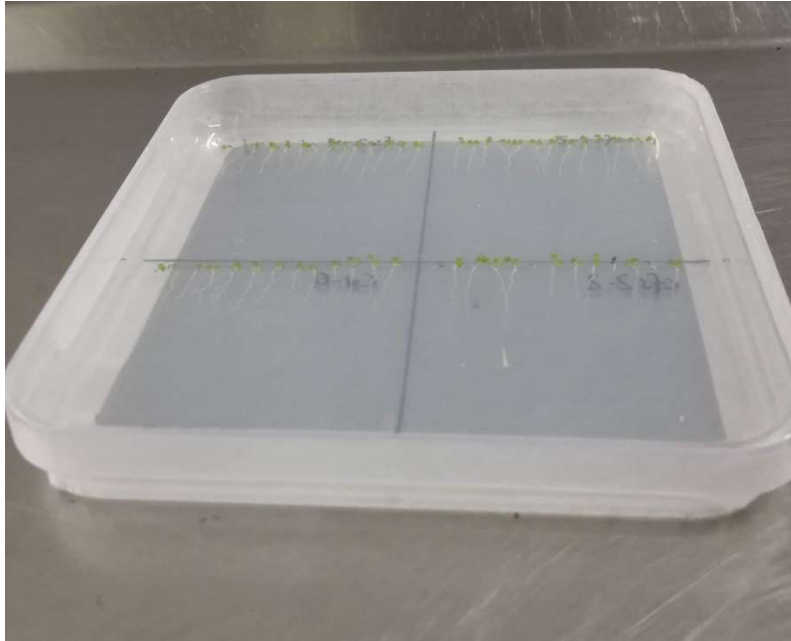


Figure 11 Roots placed on a plate are grown in a growth chamber for CM and SDCM. The optimal size was observed after the 5th day in the chamber.

When imaging with SPIM, the sample was fixated in a transparent gel block to allow the thin sheet of light to scan through the whole sample without any obstacles. The gel block was moulded into the plastic sample holder observed in Figure 13 with the help of a casting mould that can be seen in Figure 12.

- The mould with the movable plastic holder was assembled and the MS medium was mixed with Gelrite, a gelling agent, in the sterile hood.
- In order to dissolve the Gelrite, the mixture was heated up in a microwave. Approximately 40 ml of MS medium mixed with 0.4-0.8 % Gelrite is enough for two gel blocks.
- After the mixture cooled down to 80°C it was poured in and covered with glass to ensure a smooth surface.

- After 20 minutes the mould was reassembled and seeds placed in the gel attached to the sample holder.
- The gel block was then transferred to a sterile container, sealed airtight and moved to the growth chamber, where the seeds germinated.
- The roots were at perfect length for imaging at approximately 5 mm. The gel block was placed in the water bath and imaged from the root tip upwards approximately 1.5 mm.

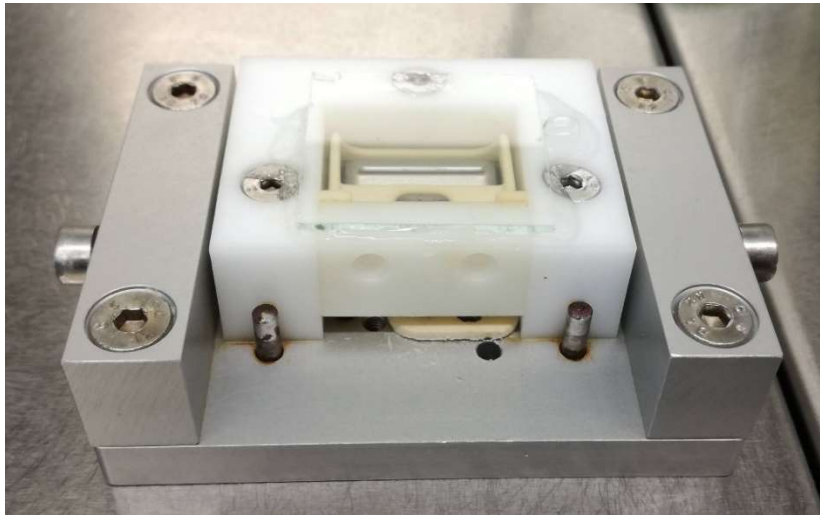


Figure 12 Mould for the gel block for the sample for the SPIM.

We used a selective plane illumination microscope that was custom made by the Advanced Microscopy Facility at the Vienna Biocenter Core Facilities GmbH. It is optimized to study plants, but is also efficient at imaging other large transparent samples. The microscope uses an illumination objective that produces a digitally-scanned light sheet of approximately 1 Hz in a horizontal plane. Its numerical aperture is up to 0.5 in air. A detection objective is located below. Its numerical aperture is 0.95 and is designed for a refractive index of 1.38. The working distance is 8 mm.

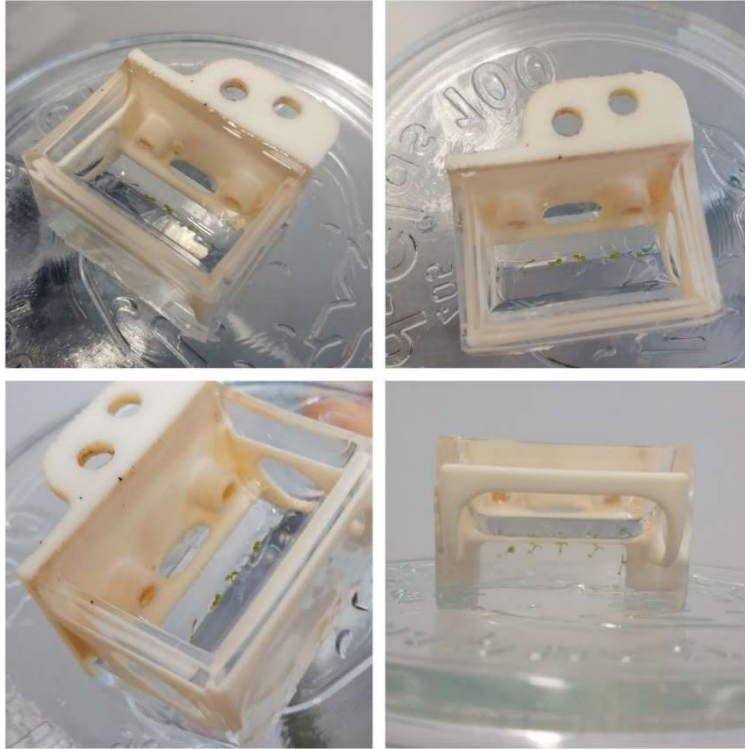


Figure 13 SPIM gel block. Seeds are placed on the gel and fully grown in a growth chamber. A hole can be created with a sterile toothpick which can assist with the straight growth of the roots.

A sample in the gel block is placed in a specially designed L-shaped sample holder that is immersed in a small bath as seen in Figure 14. The sample holder is attached to the long travel range single-axis piezo. The piezo is mounted to three DC-motors. On the right of the sample holder there is a needle that is responsible for the drainage of water to prevent water from overflowing to the sample.

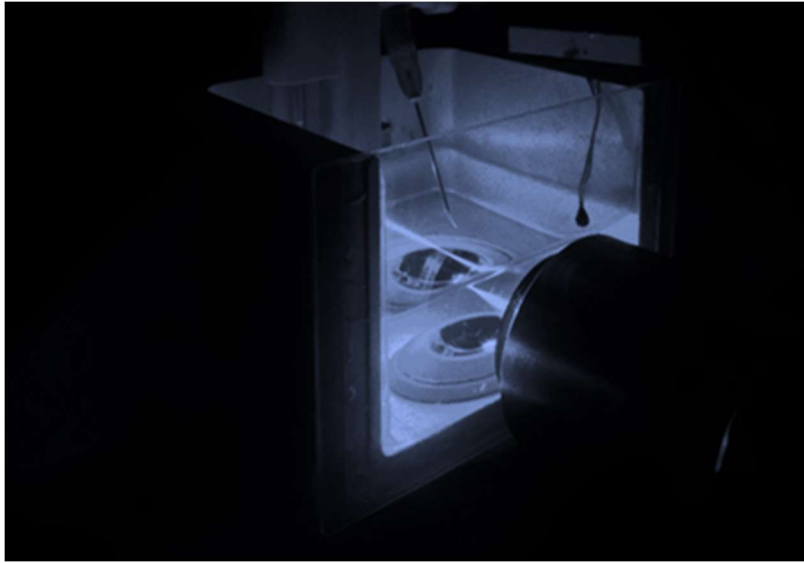


Figure 14 SPIM bath. An L-shaped sample holder is positioned on the piezo, which then moves the sample according to the pre-defined scan. The needle assists in draining the water from the sample holder, to prevent overflowing of the plants.

4.1.2 Chemical fixation

Chemical fixation was used to test the sample root. A protocol was provided by N. Fellner. Roots were taken off the medium plate and cut into pieces. They were moved to a solution of 2% glutaraldehyde in 0.1M Sörensen phosphate buffer for 2 hours in a desiccator and remained on a rotator over night at 4°C. Next day they were washed in the same buffer three times for 10 minutes. They were then moved to a solution of OsO_4 in 0.1 Sörsensen phosphate buffer on ice for 40 minutes. They needed to be washed again 3 times for 10 minutes in the same buffer. Roots were then dehydrated using the following steps:

- 40% acetone for 10 minutes on ice
- 60% acetone for 10 minutes on ice
- 80% acetone for 10 minutes on ice
- 90% acetone for 10 minutes on ice
- Twice 100% acetone for 10 minutes on ice

Infiltration and embedding followed with the following steps:

- 2 hours in 2/3 acetone and 1/3 epoxy resin
- 2 hours in 1/2 acetone and 1/2 epoxy resin
- 1/3 acetone and 2/3 epoxy resin over night
- Pure resin in desiccator for several hours
- Polymerisation for 48 hours in an oven on 60°C

4.1.3 High Pressure Freezing

After images were acquired using advanced LM techniques, the root needed to be frozen as quickly as possible for the correlation to be precise. High-pressure freezing was done with the LEICA EMPACT (LEICA Microsystems, Austria). The samples were placed on the flat gold-plated specimen carriers (2.8 mm outer diameter, 1.5 mm inner diameter, 0.5 mm carrier thickness, 0.2 mm inner wall height; LEICA Cat. #16706898).

- The carriers were placed downwards on the flat specimen holder system (LEICA Microsystems, Austria). Once ready, the carriers were picked up with a fork with the cavity facing upwards.
- It was necessary to fill the carrier with a 10% BSA solution in PBS to make sure the root would stick to it.
- The carrier containing sample was then moved with the fork towards the carrier holder where it was locked by means of a torque wrench, meaning it was squeezed between the black diamond and the carrier.
- The fork was removed and the carrier holder was attached to the loading device.
- Afterwards the sample was loaded into the high-pressure freezing system, locked and rapidly frozen with approximately 1950 - 2045 bar and cooling rates higher than 10,000 K/s.

- After the sample was frozen, it was dropped into a liquid nitrogen bath, where it was detached from the loading device and the carrier holder. After the sample is frozen, it should not be exposed to heat, therefore all the tools used were pre-cooled. Once finished with all the samples, the carriers were transferred either to the AFS or to the storage dewar. [25]

4.1.4 Freeze substitution and embedding

All the samples were then further processed by FS and embedding in the automated freeze substitution device (AFS). Two protocols were used for FS and embedding, as the workflow is divided into two intermediate techniques used for assistance with the correlation. Embedded samples can be seen in Figure 15. To retrieve the location of the autophagosomes within the root using CM, lowicryl embedding was needed to preserve fluorescence. Epoxy resin embedding was used to image the samples with μ CT to assess shrinkage and orientation after freezing. For both protocols FS was done in automatic freeze substitution system (AFS; LEICA Microsystems). The AFS should be filled with the liquid nitrogen and pre-cooled to needed temperature. The substitution medium in tubes should be placed into the AFS in the universal containers at least 10 minutes prior to the start of the program. Carriers with the samples should be moved into the AFS in liquid nitrogen and moved to the substitution medium right away. After that the automatic program can start.

Protocol for lowicryl embedding

To preserve a GFP signal in the sample we adapted the protocol published by Reipert et al. [37].

- The substitution medium contained 0.5% UA in pure acetone. The medium was pre-cooled to -90°C when the samples in carriers were added.
- FS was then performed at this temperature for a minimum of 2 days. After FS the temperature was gradually raised

with the help of the automatic system up to -40°C . The exact temperature increments can be found in Table 1.

- Once this temperature was reached, the samples needed to be washed with pure acetone three times. All of the further steps were done inside of the AFS at -40°C .
- After washing, the samples were infiltrated with the different mixtures of lowicryl HM20 and acetone.
 - First step was in $1/3$ lowicryl HM20 and $2/3$ acetone mixture for 30 minutes.
 - Second step was in $1/2$ HM20 and $1/2$ acetone mixture for an hour.
 - Third step was in $2/3$ HM 20 and $1/3$ acetone mixture for 2 hours
 - Last step was in pure lowcrylic HM 20 for another hour.
- Infiltrated samples were then transferred in their carriers into the lids of the PCR cups that were pre-cut to be fit for the spider net. The lids were filled with a drop of fresh pre-cooled resin and the carrier was inserted with the cavity facing upwards.
- The tube from the PCR cups was pressed onto the lid and filled up with the fresh resin. It was then mounted on a holder called spider cover, which was then placed on the stem holder to keep it floating.
- The AFS is then covered with the UV light and the polymerization continued for 24 hours at -40°C . The samples were then warmed up to room temperature. The gold-plated carrier was removed with the help of razor blade and trimmer.

Table 1 HM20 UA protocol for AFS with temperature steps. In step 6, samples are embedded and afterwards polymerized with addition of UV light.

Steps	Starting temperature in °	Ending temperature in °	° per h	Time in h	UV
1	-90	-90	0	31	
2	-90	-54	3	12	
3	-54	-54	0	8	
4	-54	-40	1.5	9:40	
5	-40	-40	0	6	
6*	-40*	-40*	0*	1*	
7	-40	-40	0	48	X
8	-40	10	10	5	X
9	10	10	0	3	X

Protocol for epoxy resin embedding

Using a substitution medium of 2% OsO_4 in pure acetone showed good results in TEM but the contrast was too little for μ CT, therefore we added UA (0.5%) when preparing samples for the μ CT.

- Once the sample carriers were added into the tubes containing the pre-cooled medium, the FS at -90°C took place for at least 48 hours. Exact temperatures can be found in Table 2.
- Afterwards the temperature was gradually raised to 0°C . When preparing the samples for the μ CT, AFS was warmed to room temperature and the samples were left within the device for another hour.
- The samples were washed on ice three times with acetone with 10 minutes breaks.
- The samples were infiltrated with different concentrations of epoxy resin.
 - First step was in 1/3 epoxy resin and 2/3 acetone for 6 hours.

- Second step was 1/2 epoxy resin and 1/2 acetone overnight.
- Third step was 2/3 epoxy resin and 1/3 acetone for 6 hours.
- Transfer the samples in pure resin overnight.
- The carriers were placed facing upwards into the tube with a drop of resin, then half filled and left in the exsiccator for 2 hours.
- Lastly, they were polymerized in the oven at 60°C.

Table 2 Temperature increasing steps during FS for embedding in epoxy resin. Step 7 was performed when samples were prepared for μ CT imaging.

Steps	Starting temperature in °C	Ending temperature in °C	° per h	Time in h
1	-90	-90	0	41
2	-90	-54	2	18
3	-54	-54	0	8
4	-54	-24	5	6
5	-24	-24	0	15
6	-24	0	6	4
7*	0*	0*	0*	1*



Figure 15 Polymerized HM20 samples on the unique spider web, which assists with the polymerisation, as the UV light is able reach the sample from all the sides, including the bottom. On the right: epoxy resin embedded trimmed sample.

4.1.5 Sectioning

Once the resin polymerized, we trimmed the carrier away with the help of a Leica EM Trim (LEICA Microsystems, Austria). Using a razor blade, we removed the remaining parts of the carrier from the sides. Afterwards, we trimmed the rest of the surrounding resin to prepare the sample for sectioning. Sectioning was done using the Leica Ultracut UCT Ultramicrotome (LEICA Microsystems, Austria). Different thicknesses were cut for different purposes. When sectioning for CLEM, sections were thicker (≈ 150 nm) and when sectioning for TEM the ideal thickness was 70 nm. After the desired thickness was achieved, the room was left until a line of sections such as in Figure 16 was obtained. The sections were afterwards placed on grids.

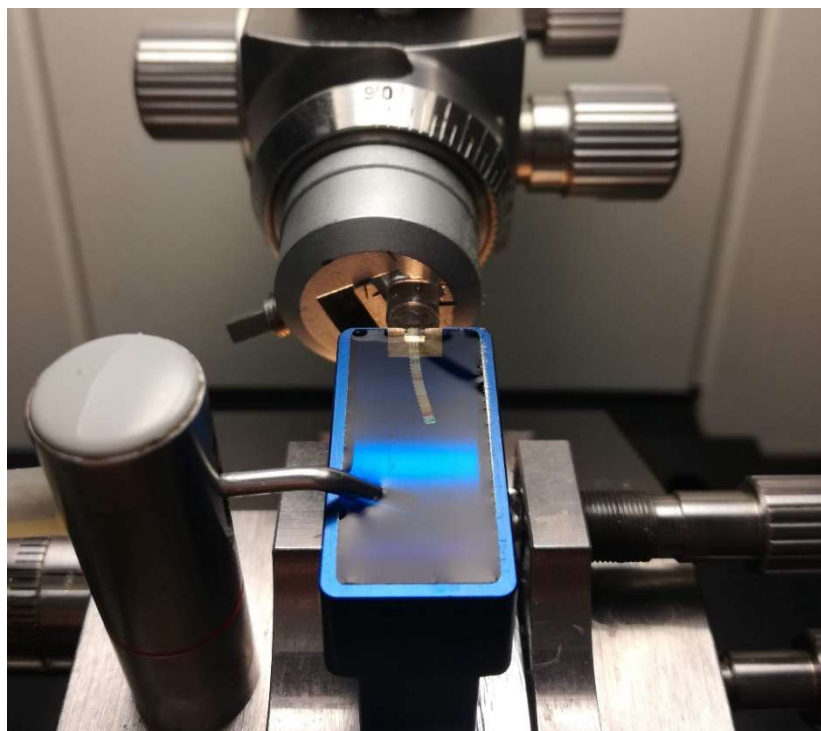


Figure 16 Sectioning a sample to 70 nm slices to put on a grid and image with TEM. This is the final step in the workflow with μ CT, as for CLEM, thicker samples are needed in order to observe fluorescence.

4.1.6 CLEM

We imaged both samples embedded in epoxy resin and in lowicryl HM20 resin. For CLEM we used both the conventional confocal microscope as previously described in the workflow and a Leica EM Cryo CLEM system, without using the cryo-option. All samples were handled at room temperature. For imaging with the Zeiss confocal microscope (SPIM780 Carl Zeiss MicroImaging GmbH, Jena, German), the grid was placed on the glass slide with a drop of distilled water and covered with a cover slip. When imaging with the CLEM system, special handling of the grid was in place. To insert the grid into the microscope a special transfer shuttle (LEICA Microsystems, Austria), as seen in Figure 17, was used.

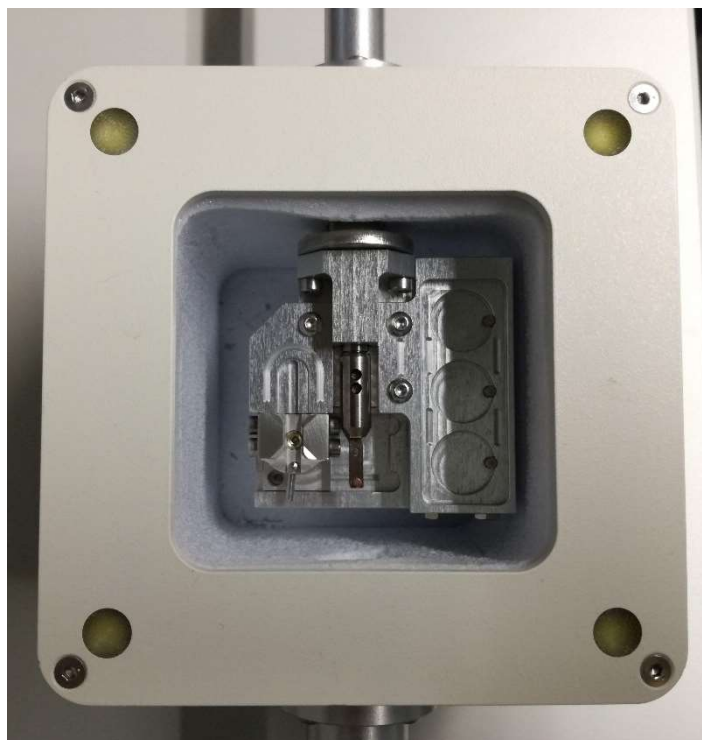


Figure 17 Leica transfer shuttle. The grid is inserted in a thin copper sample holder with the assistance of this device. The device and sample holder are then attached to the CM. The sample is then inserted into the microscope. If needed, samples can be imaged under cryo-conditions. In our case, that was not needed.

The grid is placed onto a thin copper sample holder that is picked up and inserted into the microscope. The imaging is done with the help of Leica software, with which it is possible to mark regions of interest and landmarks to be found again when imaging with other techniques. Once the grid is viewed in the TEM, the program Serial EM can be used for finding the positions again. The CLEM system is only compatible with FEI Tecnai G2 20, a 200 kV TEM equipped with an Eagle 4k HS camera which includes Serial EM.

4.1.7 Post-Staining and imaging with TEM

Grids with sections on them were post-stained using Reynold's lead citrate and a 2 % UA solution. Both vials were microcentrifuged at maximum speed for 10 minutes. Small drops of UA were placed on a

prepared parafilm. On each drop one grid was placed, section facing downwards, for 10 minutes and was covered with a petri dish wrapped in aluminium foil. The grids were then picked up with a forceps, rinsed thoroughly with double distilled water and dried with a piece filter paper from the side of the grid. They were then placed on prepared drops of Reynold's lead citrate surrounded by several pellets of NaOH around the edge of the parafilm. They were covered with a petri dishe to prevent air exposure and left for 5 minutes. They were then picked up with a forceps and rinsed with double distilled water and dried with a filter paper again. The grids were placed in a grid box and left there to completely dry up after post staining. Afterwards, all imaging was done using 100 kV FEI Morgagni 268D operated at 80 kV, equipped with an 11 megapixel CCD camera.

5 Results

When first starting the project, the samples had not been imaged by SPIM, μ CT or TEM before. It was necessary to test and optimize all modalities and adjust the sample preparation protocols accordingly. Once satisfying results were obtained, the workflow to correlate the techniques was adjusted.

5.1 Imaging modalities

5.1.1 SPIM

After first experiments with SPIM, a brighter root tip and blurry centre was observed as seen in Figure 18. The image quality was insufficient to visualize the location of the autophagosomes, except for the outer layer of the root. As seen in the figures below, the tip of the root was brighter than the rest, and signal was lacking from the structure in the middle.

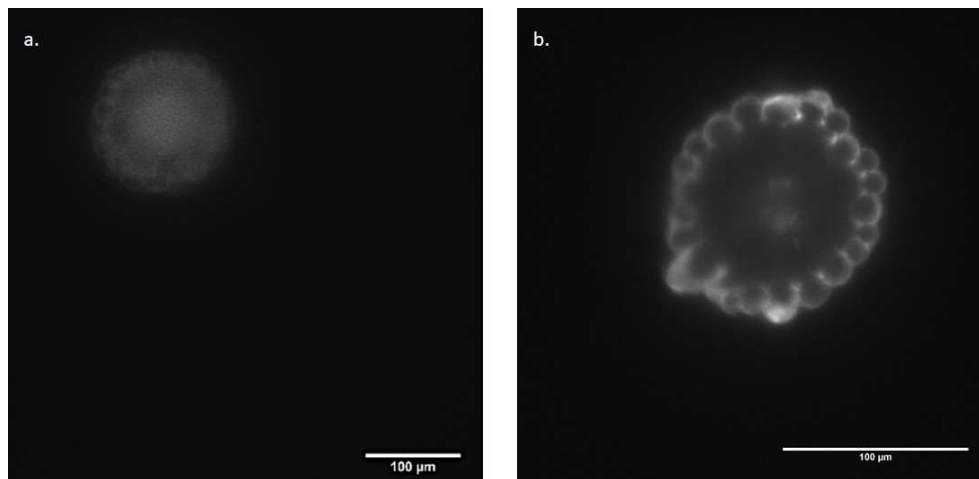


Figure 18 On the left (a), we see a bright tip, brighter than the rest of the root. On the right (b), the structure within the root is missing. These results were found to be insufficient for the purpose of this project, therefore multiple attempts were done to improve the quality.

Multiple optimization steps were taken to improve image quality. A different gel was used, which, if older, would have a different refractive index leading to blurred signals. However, the same results were observed. The roots were then imaged solely on a coverslip without agarose embedding. Results did not improve as the incline of the root resulted in an even blurrier image. Results did not improve either after increasing the labelling density.

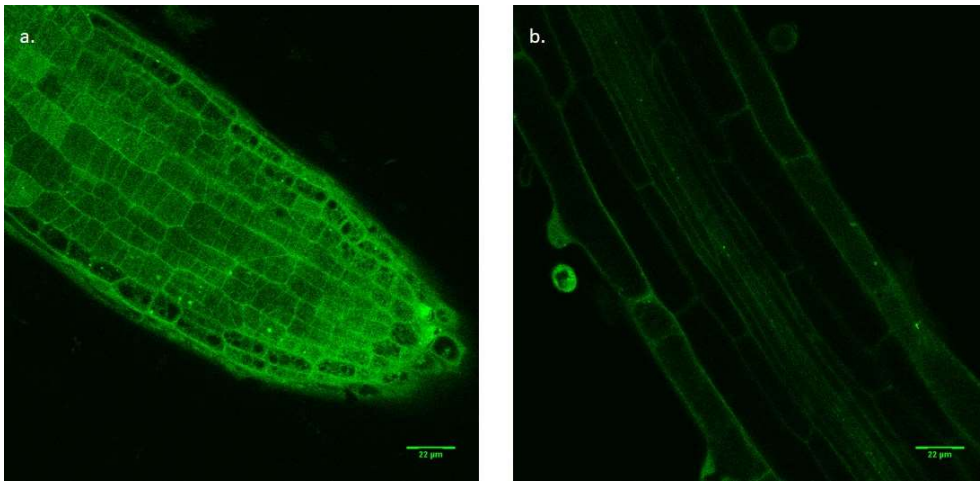


Figure 19 CM visualized the inner structure of the sample in the middle and at the tip of the root. Autophagosomes can be seen both in the middle and the tip of the root.

Imaging the exact same root with CM, the tip and the centre of the root were clearly visible (Figure 19). Modifications of the system were done by Advanced Microscopy facility and changing the width of the light sheet resulted in improved image quality and therefore it was decided to proceed with the correlation attempts. After modification, it was observed that the image quality improved drastically if the root grew straight rather than curved. The root tip remained brighter than the rest of the root as seen in Figure 20. Autophagosomes were observed in the centre of the root after the optimization, but they were best seen

in the root hair, which is why root hair cells were used for further correlation workflows.

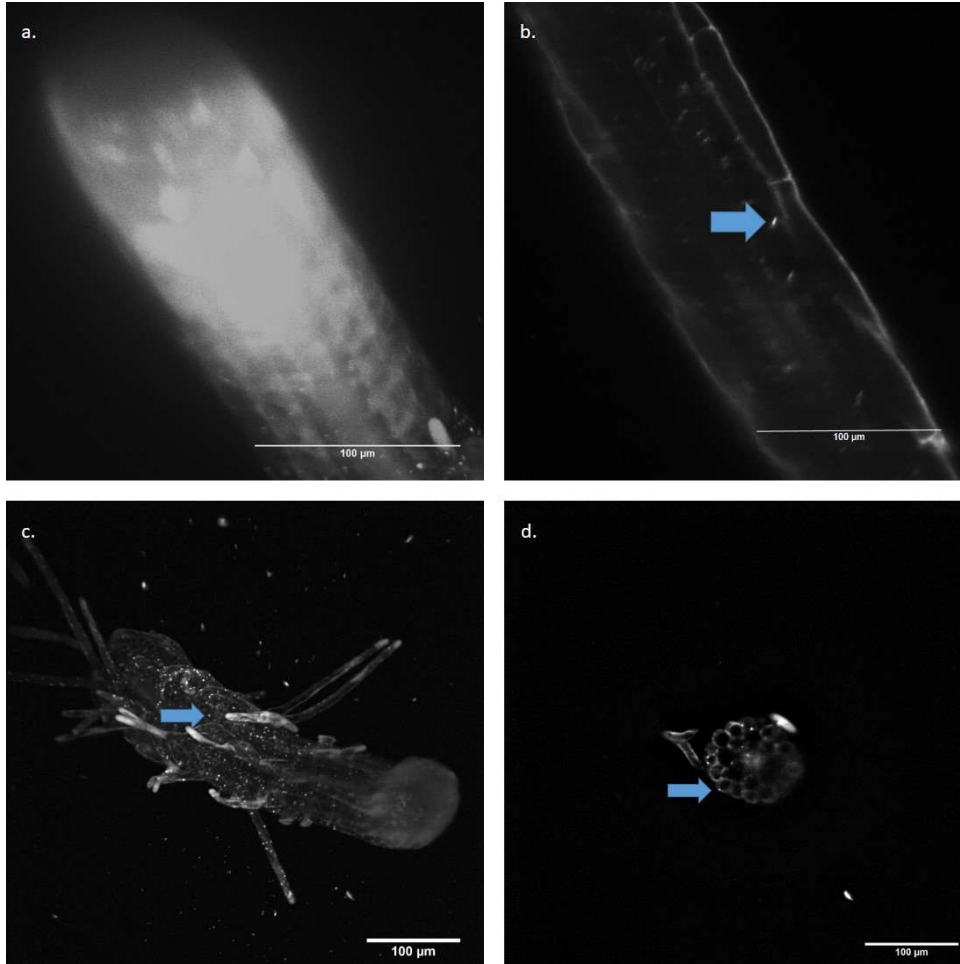


Figure 20 The root tip remained overly bright even after the modification as can be seen in a. and c. We believe the reason for this is the cell size in the tip and the amount of the GFP-labelled ATG8 A protein. Autophagosomes were observed in the middle of the root after the modification as seen on b. and d.. They are marked on the image with blue arrows. Overall image quality was improved.

5.1.2 CM

The CM signal was clear and image quality was sufficient for our needs (Figure 21), however, scanning time with CM is long. To obtain a z-stack of the root in good quality, it can take up to a few hours, dependent on the desired quality. Within this time, in living organisms the structure can change drastically and what we see in our confocal image will be long gone before we get to high-pressure freeze it. This

makes correlation unfeasible. Autophagy is a fast process and autophagosomes are created and digested within minutes.

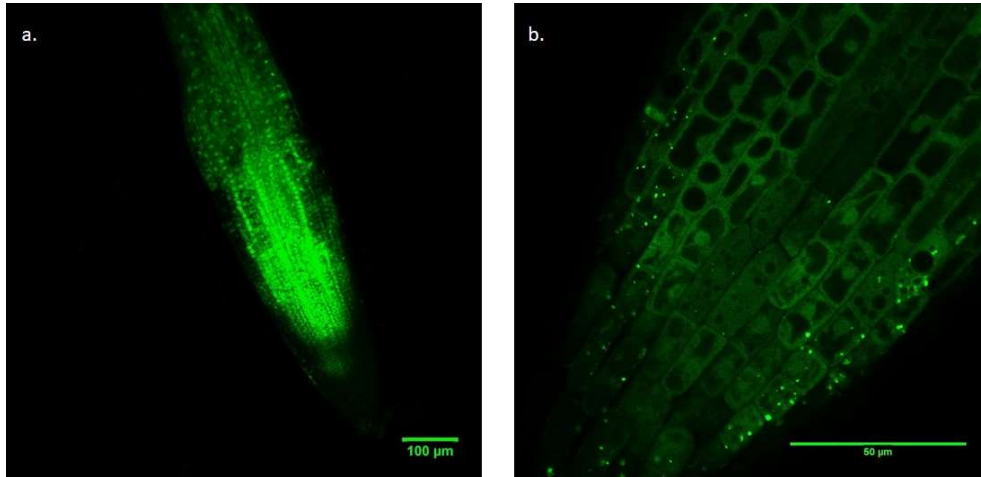


Figure 21 CM gives good results when imaging autophagosomes, however a high-quality z-stack, which we need for the co-alignment, would take too long to scan. However, CM was a useful tool when we were checking our samples and the GFP signal.

Even though scanning living roots was not an option, CM was used as an intermediate step to re-locate our region of interest within the root and re-identify autophagosomes. As expected, embedding the sample in epoxy prevented the detection of a GFP signal and quenched the fluorophore (Figure 22). However the samples embedded in HM20 preserved the signal. We observed that after a longer period of time, the fluorescence would almost completely disappear. Best results were obtained when imaging the sample the same day. The Leica CLEM system we used had limited magnification, which did not allow to visualize autophagosomes. Further experiments were done with a Zeiss confocal microscope. We also observed that in sections of only 70 nm, the signal was too weak to observe. Best fluorescent sections were about 250 nm thick or thicker.

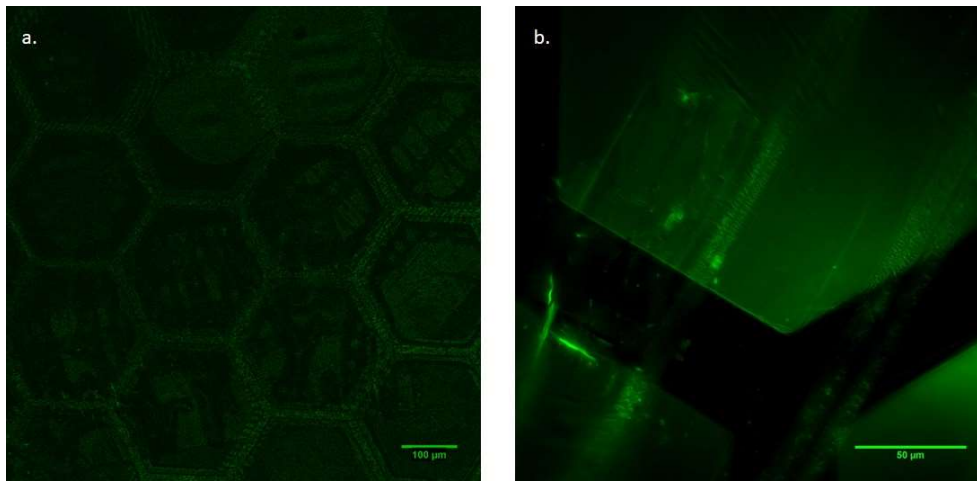


Figure 22 We used CM as an intermediate step for visualizing the sample after it had been embedded. Fluorescence is lost after epoxy-resin embedding without any detectable structure (a). On the right (b), cell walls and brighter dirt spots can be observed.

5.1.3 SDCM

While conventional CM was not fast enough for live-imaging, spinning disk microscopy was used. Scans take only few seconds, and an entire 3D root stack was acquired within seconds. Multiple exposure times were tried out on the same root to identify ideal settings for best image quality. Longer exposure time were preferred over shorter exposure as the image quality using shorter exposure time was not sufficient as seen in Figure 23. In image a, the exposure time was 50 ms and the scan took only 4 seconds. However, the image quality was too low to distinguish autophagosomes from noise. With an exposure time of 200 ms, autophagosomes were seen more clearly, as seen in image b. The scan took 16 seconds. On the images c. and d., exposure time was 500 ms, but two different cameras were used. Better results were seen when using the sCMOS camera on the right, but the EMCCD camera was sufficient as well. The scan with the EMCCD camera took 50 s while the scan with the sCMOS camera took only 36 s. Best results were obtained with exposure times of 500 ms with the sCMOS camera.

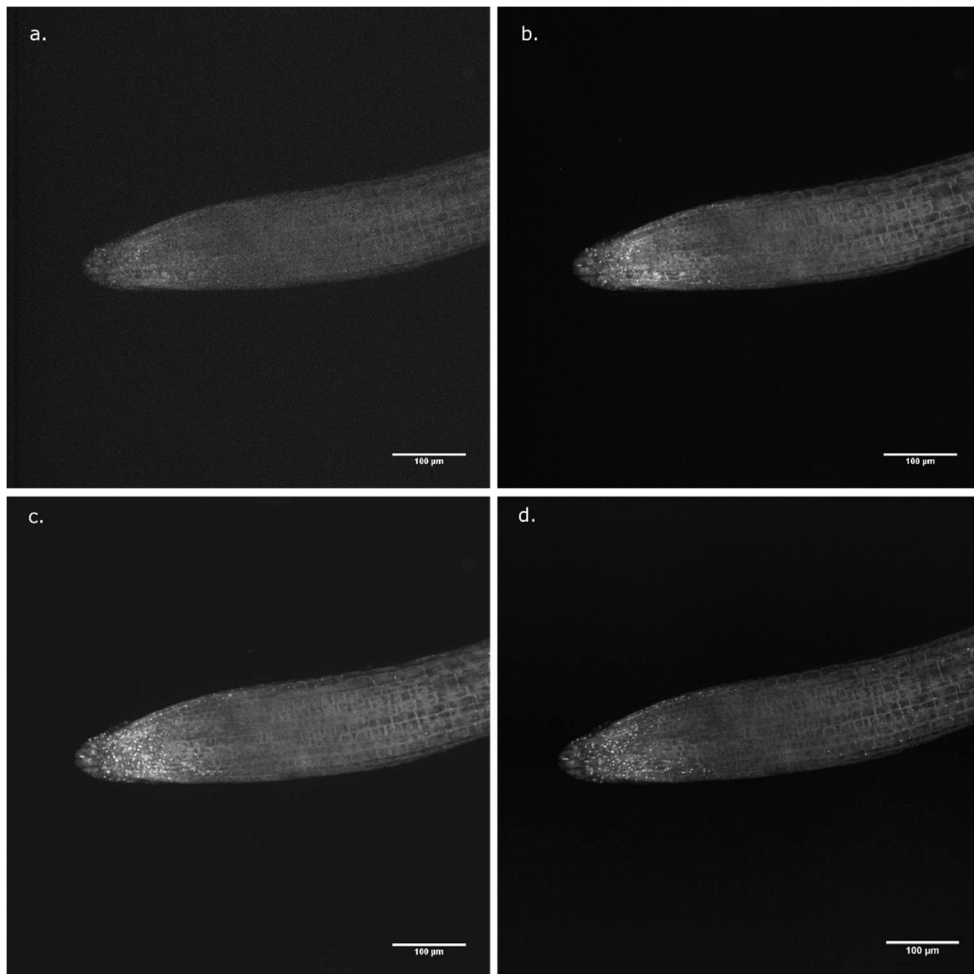


Figure 23 Differences between exposure times (50, 200 and 500 ms). Exposure times were compared on the same root within 5 minutes. Best results can be observed in c. and d., where the autophagosomes are clearly distinguishable from each other.

As in SPIM, in Figure 24, we can observe slightly stronger brightness in the tip and less clarity in the middle of the root.

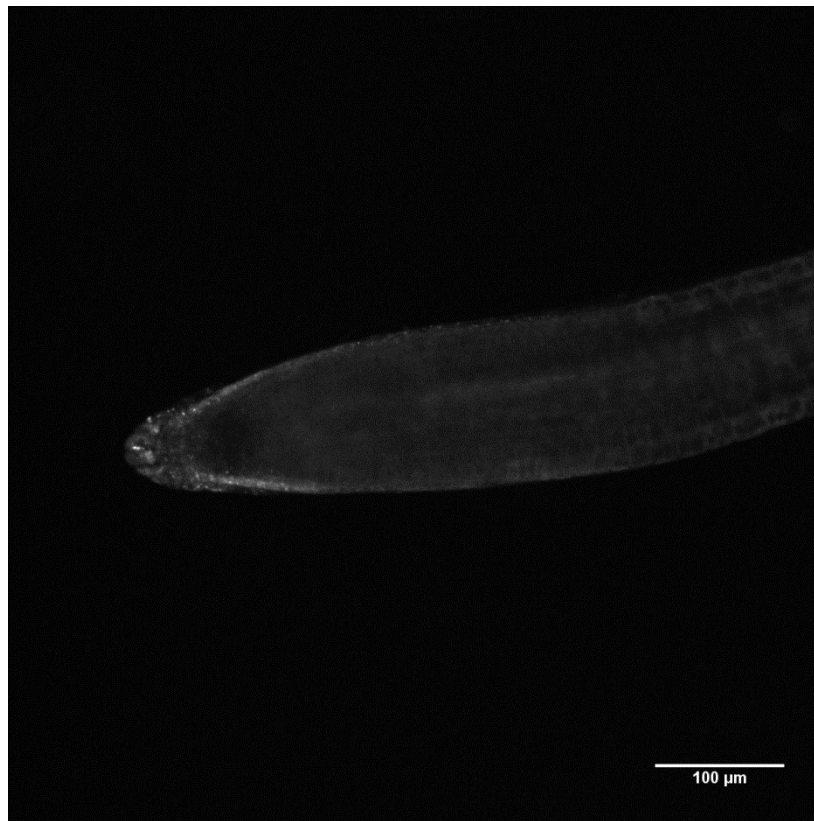


Figure 24 The tip of the root and the middle are blurry and without structure. This is improved by increasing the exposure time.

5.1.4 μ CT

μ CT was added to this project as an intermediate step to assess shrinkage after fixation of the root and to verify the orientation of the root within the embedding medium. The root was stained with UA and OsO_4 to enhance contrast for the μ CT scans.

Roots were first imaged after chemical fixation, to test if the resolution and contrast are sufficient. The contrast was low, nevertheless, as seen in Figure 25 some structure within the root was visible. Surely, shrinkage and orientation can be determined.

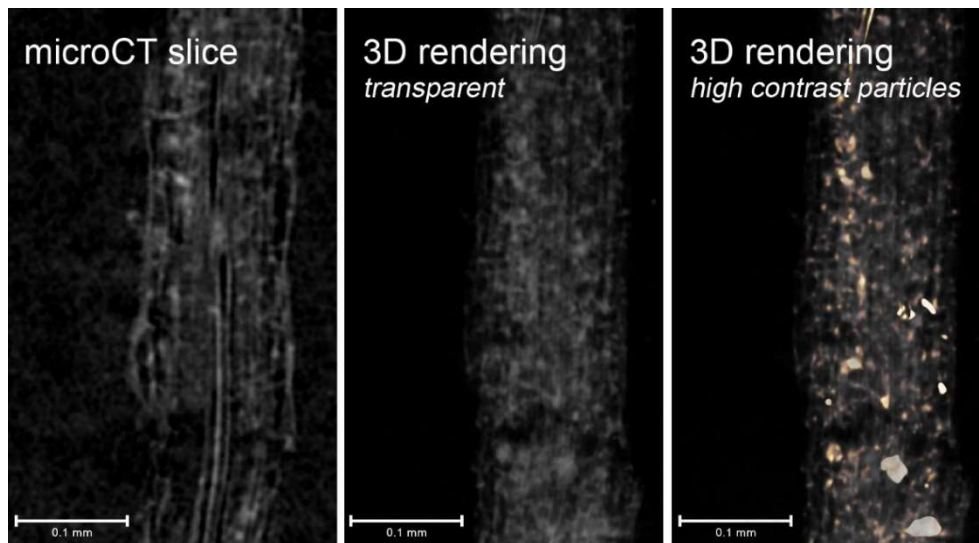


Figure 25 Results from imaging the chemically fixated root were better than expected, the structure can be observed within the root. There are also some structures that are higher in contrast, which was at first believed it could have been autophagosomes. That hypothesis was later disproven.

Some unknown round structures were seen in the CT scans. To verify whether these structures are autophagosomes, a root with autophagy deficiency was imaged - which would exclude these structures as autophagosomes if observed again. Similar structures were present in the autophagy-deficient root as well which makes the nature of the structure unknown.

Since the signal was not very strong, attempts were made to increase staining. However, even after leaving the samples in osmium tetroxide for additional hour on room temperature, the staining was too faint and it resulted in low contrast. Afterwards the protocol with FS medium containing 0.5% UA was used, nevertheless the results remained unchanged so further optimizations will be needed before we detecting autophagosomes. Nevertheless, using μ CT to assess shrinkage has become a feasible option.

5.1.5 TEM

The project involved establishing and optimizing a variety of imaging and sample preparation protocols. One of the first protocols

established for the roots was its chemical fixation to see if the sample is well preserved in TEM. Results were good, but - as we can see in Figure 26 - the membranes of the vacuoles are more curvy than usual and cell walls are not as smooth as they are in ideal conditions. However, the ultrastructure of the root can be observed well. Membranes are intact and other organelles can be clearly spotted.

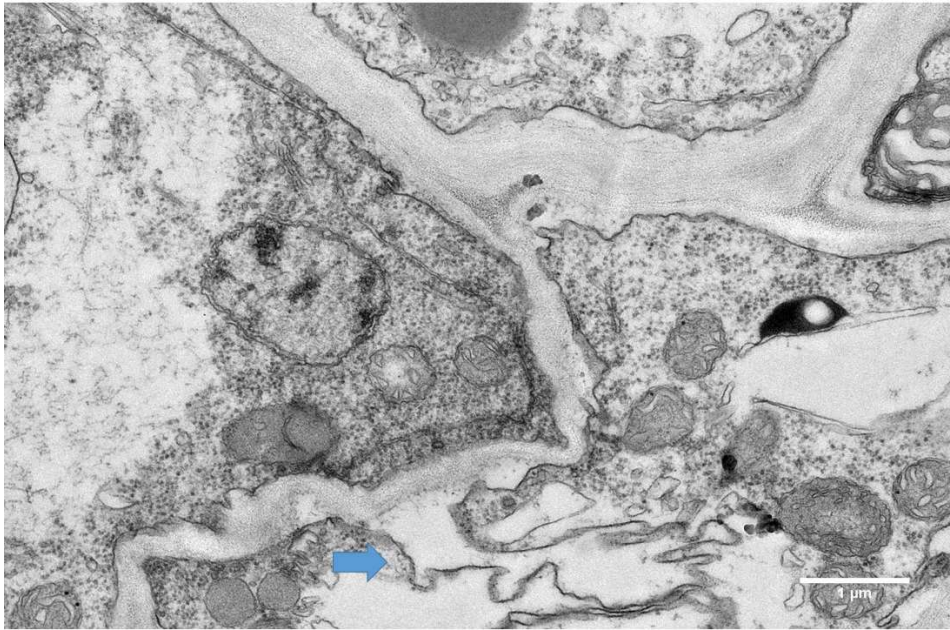


Figure 26 Chemical fixation is a well-established way of preparing a sample for TEM observation. The results that were observed with roots were as expected: We can see that intracellular structures are well preserved, but that the cells are deformed and that the membranes are not completely smooth as seen next to the blue arrow. HPF was selected as a preferred fixation.

As double-membrane autophagosomes are the object of interest, membrane preservation is of utmost importance. HPF showed good results in the past, with the advantage of fast fixation of intracellular activities. [20]

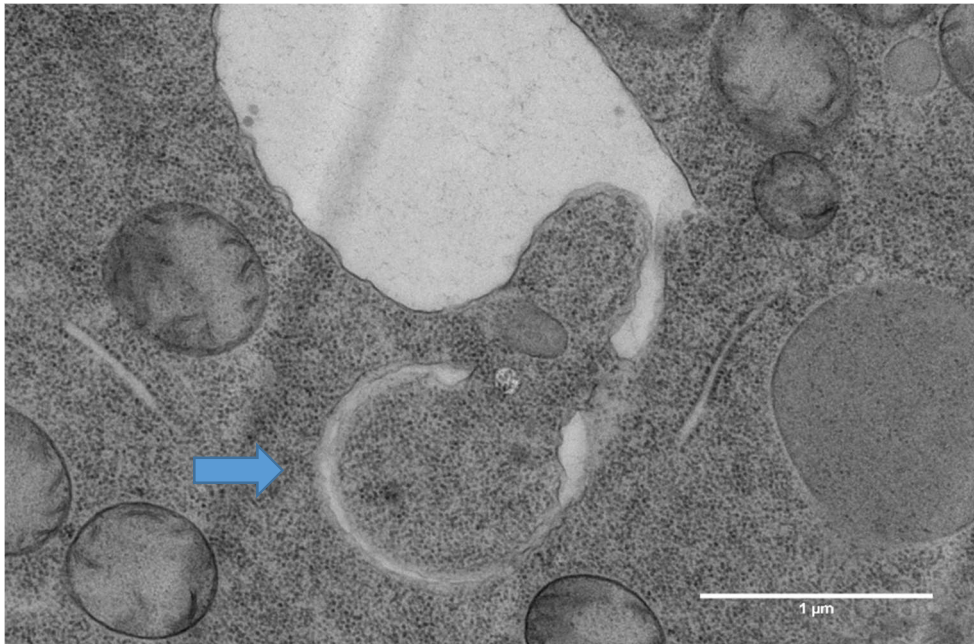


Figure 27 HPF and epoxy embedding showed good results, cell shapes were not compromised and the membranes were well preserved. We can observe a phagophore moments before completing the circular structure marked with a blue arrow.

Multiple FS mediums were used. Best results were observed when performing FS in acetone and osmium which can be observed in Figure 27. We can see good preservation of other cellular organelles as well, such as the mitochondria next to the autophagosome.

Using epoxy resin after FS in the substitution medium solution also showed good results. UA would not have been added to the medium if it were not for μ CT, which required stronger staining steps. Results in TEM were not better than with FS using a substitution medium containing only OsO_4 .

The aim of using HM20 was the preservation of fluorescence. Initial results for HM20 embedding looked promising, but could be improved (Figure 28).

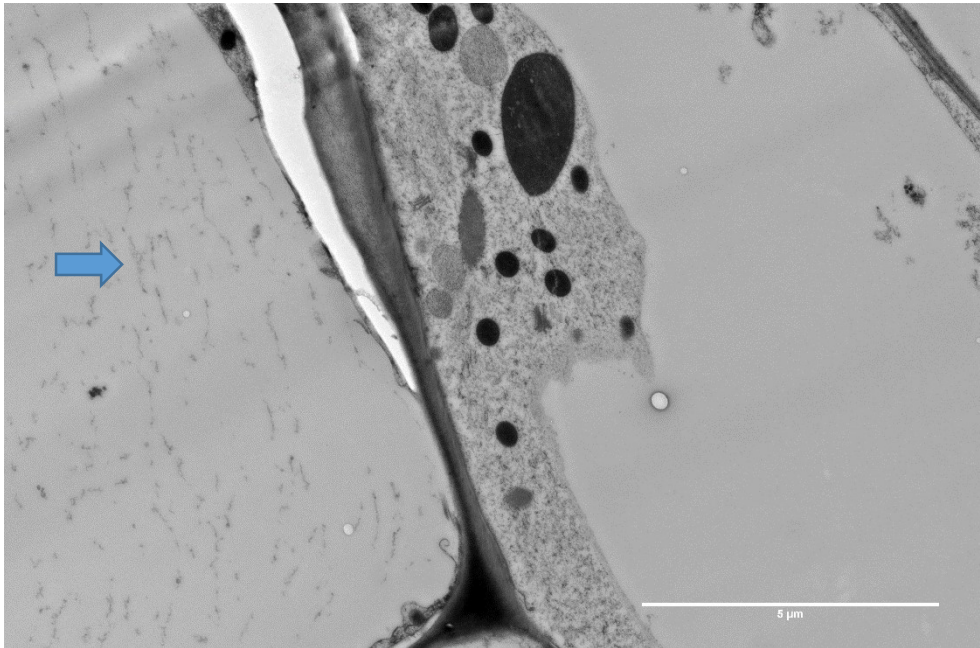


Figure 28 High-pressure frozen sample embedded in a lowicryl HM20 resin, results were not optimal at first. There were particles in vacuoles marked with a blue arrow that are usually not observed, and membranes were not intact.

The reason for this could be exposure to heat, which can result in immediate crystal formation in the sample. The membranes were not intact and cell components were not easily identified. Results were improved over time and got almost as good as those obtained with resin embedding (Figure 29): Membranes were easy to observe although not perfectly preserved. Additionally, nuclei, potential autophagosomes and mitochondria could be identified (Fig. 29).

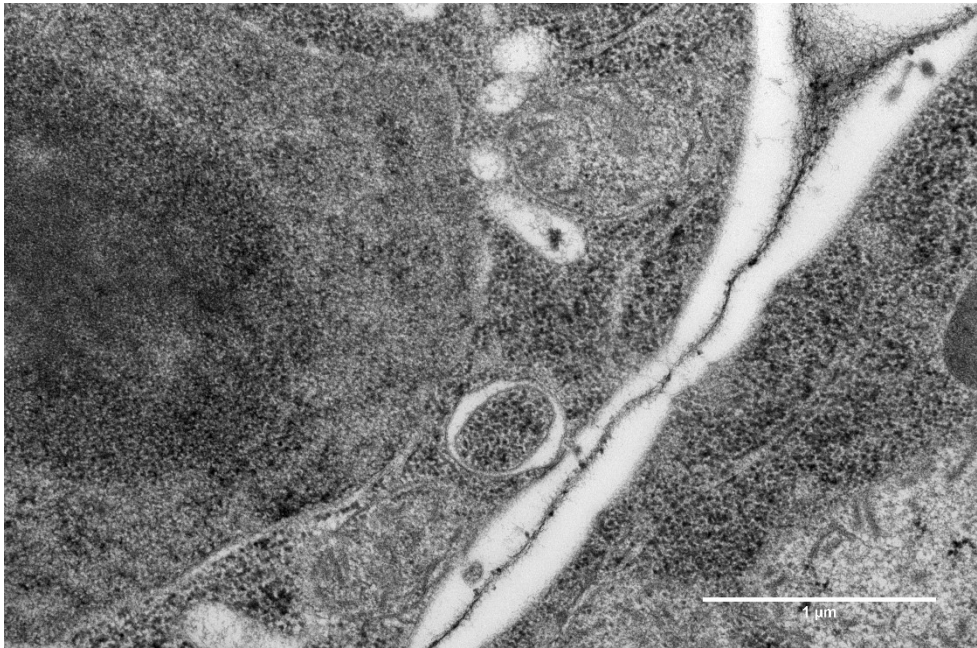


Figure 29 The HM20 protocol on the second try resulted in a much better quality. We can observe an autophagosome, a double membrane vesicle near the cell wall and the nucleus.

Most autophagosomes observed were found close to cell walls. This is not surprising since vacuoles take up most of the space inside the root. In many cases autophagosomes were observed close to the nucleus, as seen in Figure 30, which strengthened the hypothesis that autophagosomes are created from the nuclear membrane.

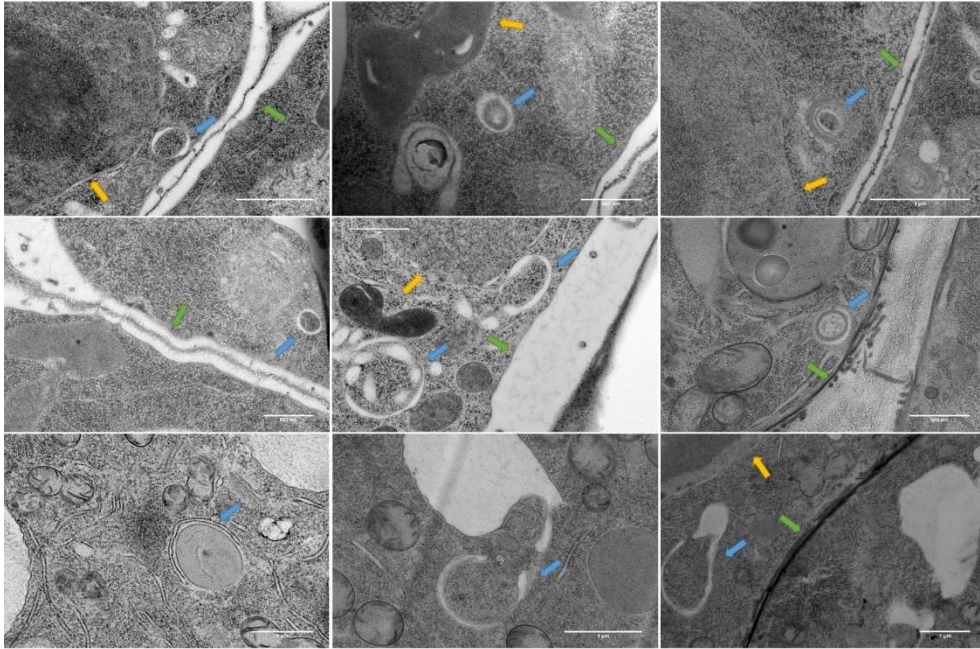


Figure 30 Blue arrows point to autophagosomes, yellow arrows point to the nucleus and green arrows to cell walls. Scale bar size varies between 500 nm and 1 μ m. Many of the autophagosomes were seen near the nucleus and cell walls. Autophagosomes were observed in different stages, from the phagophores to degrading singular membrane vesicles in the vacuoles. The best way to verify whether the identified structures were indeed autophagosomes is correlation.

5.2 Correlating modalities

Correlation was tackled after the optimization of the protocols. Several correlative workflows were carried out, either following the SPIM or SDCM. A few roots were lost during HPF and freeze substitution. Nevertheless, five successful rounds of the established workflow were carried out using SDCM and three using SPIM. Three of the SDCM imaged roots were used for the correlative workflow including μ CT and two for correlating with CM. One root imaged with SPIM was stained with osmium and UA for correlation with μ CT and the other two were embedded in HM20. Both correlative workflows and their variations are at the forefront of correlative imaging since, worldwide, to our knowledge, they have not been demonstrated before.

5.2.1 SDCM, CLEM and TEM

After performing SDCM, roots were transferred from coverslips to the carriers to perform HPF. This needed to be done quickly, as roots are dynamic organisms and autophagosomes are disintegrated within minutes. The whole transfer from SDCM to the high-pressure freezer was done in less than four minutes, which might still be too slow for capturing all autophagosomes seen with LM. After freezing, samples in liquid nitrogen were moved to the AFS where the FS protocol for preserving fluorescence was performed. After three days, the samples were embedded into HM20 lowicryl resin and polymerised under UV light. A resin block was sectioned, and sections laid onto the grid. At first a finder grid with no coating was tried out, however the sample did not remain on it. Therefore, a carbon coated formvar grid was used. After observing the grid with CM, the same grid was imaged with TEM. In Figure 31, images of all three modalities of exactly the same sample and same region can be observed, however the exact slice still needs to be located within the entire 3D volume.

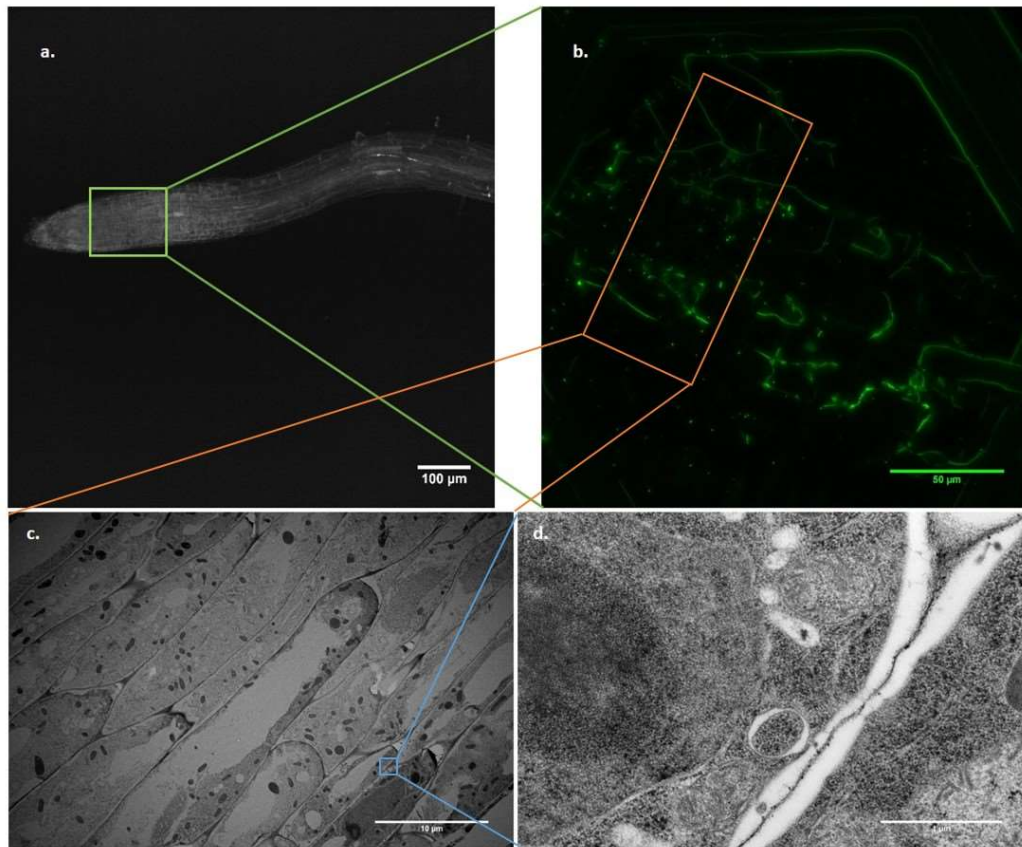


Figure 31 The first image was taken with SDCM, after which HPF was performed. Image b. highlights cell walls and brighter spots that were not unambiguously identified. For validation, a better resolution and preservation for TEM would be required.

5.2.2 SDCM, μ CT and TEM

When correlating with μ CT, the FS protocol for embedding in epoxy resin was used. Because, at first, the contrast was weak, the roots were stained in OsO_4 for additional hour at room temperature. As seen in Figure 32.b, autophagosomes were not detected, but the shape of the root is visible. To align the two images from CM and TEM, some reference structure will be needed. The outline of the root tip might serve as a rough coordination template for further correlation. Importantly, the outlines visualized with μ CT can help to access and quantify overall shrinkage for a precise correlation after fixation.

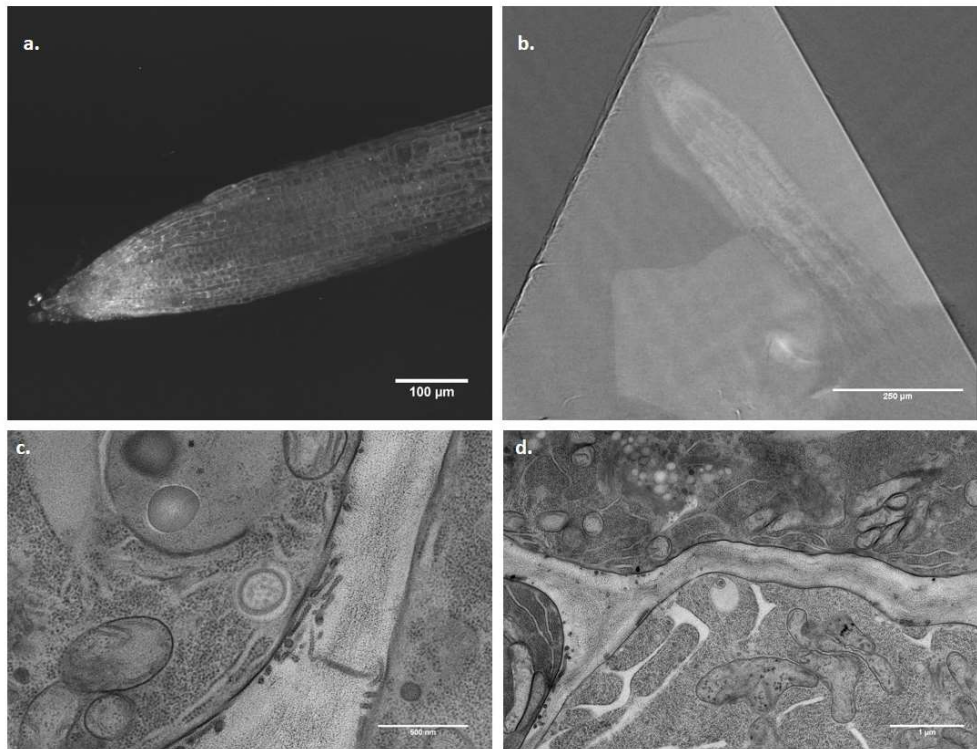


Figure 32 The first image is taken with SDCM and we can observe the same root with μ CT (2D projection shown). In (c) and (d), the root was observed with TEM. The μ CT image did not visualize enough details to correlate and assess the shrinkage and orientation.

5.2.3 SPIM, μ CT and TEM

Two of the roots imaged using SPIM were embedded in epoxy resin following a stronger staining protocol after HPF. We used a FS medium containing UA and OsO_4 and added an additional hour of staining at room temperature to our protocol to achieve higher contrast for the intermediate step of μ CT. A longer staining period did not improve the contrast in the μ CT, as seen in Figure 33, but the root outlines observed by μ CT might be used in future to assess root shrinkage.

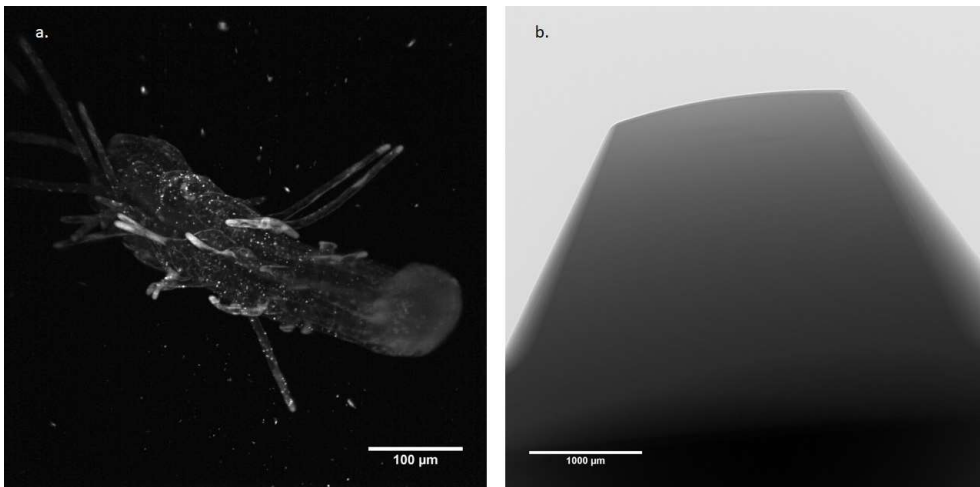


Figure 33 On the left is SPIM image of the same sample that was embedded into epoxy resin using the protocol for stronger staining. Root was hardly visible with μ CT (b.), therefore another staining protocol will be needed.

6 Conclusion

In recent years, autophagy in plants has been researched extensively, however the discovery of autophagy selectivity in plants generated a need for further investigation of responses to stress conditions and the advanced machinery of ATG8s. This project has used five imaging modalities with the motivation to assist in understanding autophagy in plants further. By addressing autophagy, we established a novel correlative workflow used to observe autophagy with a high potential to be used to address other unanswered current biological research questions. The chosen modalities were proven to be appropriate to tackle autophagy in plants. SPIM and SDCM were selected to address the role of autophagy in plant development. They have the advantage of quick acquisition time which is beneficial for the correlative workflow, due to the fast intracellular changes in living organisms. To visualize the same sample and correlate the autophagosomes, the time window is the length of the autophagosome degradation, therefore only a few minutes. The occurrence of autophagosomes in dependence to stress conditions and cell type within the overall living root was of particular interest. Longer time series can be acquired with SPIM, therefore different stress conditions can be tested and visualized on the same sample. An *Autophagy atlas* that describes the cell-type specific occurrence of autophagy in control conditions for ATG8 A GFP labelled *Arabidopsis* root was created using these two techniques. Due to no stress, autophagy was less present. Nevertheless, autophagosomes were visualized well, especially in the root tip and root hair. To assess biogenesis and preferred location of these autophagosomes within their specific cell type, we used TEM. μ CT and CM were utilized to facilitate the correlation and the re-identification of areas/autophagosomes of interest, quantifying shrinkage and determining the orientation of the root within the embedding medium.

Protocols have been established and optimized for all imaging modalities and sample preparation steps - which lays the basis for

further implementation of correlative workflows to tackle autophagy in plants.

Several modifications were necessary to achieve image quality. For SPIM, the light sheet thickness needed to be adjusted which then improved detection within the root. The GFP-labelled protein ATG8 A is denser in the root tip and therefore produces saturation during imaging. For SDCM, image quality was sufficient in our first trial, and once the exposure time was chosen, we started to work on the correlative workflow. The CLEM system required several modifications as thinner sections had a reduced signal and were difficult to visualize. Additionally, photo bleaching occurred rapidly when imaging these thin sections. Nevertheless, best image quality was achieved by increasing the thickness of the sections and by imaging sections the same day they were sectioned and placed on the grid. For TEM, it was difficult to identify autophagosomes within the cell. Research results about autophagosomes published in [34], [38] helped with the identification. TEM protocols were optimized for best image quality and sample preservation. In many cases autophagosomes that were visualized with TEM were located near nuclei and cell walls. As it is still uncertain, where within the plant cells autophagosomes are created, this is a valuable observation. For the validated localization of autophagosomes, correlation is the method of choice. First correlative workflows have been successfully established. However, the co-alignment of images still needs improvement and automated localization algorithms to say with certainty that what we observed with TEM is indeed what we observed with one of the advanced light microscopy techniques.

Both correlation workflows may result in full correlation, although until correlation algorithms are applied, it is hard to predict which one would provide a better outcome. The publication by Handschuh et al. [39] correlates μ CT and TEM and documents this well. Nevertheless, μ CT of resin embedded roots is not yet explored. We believe the reason for the low contrast might be the large concentration of water within roots. Cells mostly consist of vacuoles which is why all cellular

organelles can be found next to the cell walls. This leaves little area to stain and therefore could be problematic during visualization with μ CT, whose maximal resolution amounts to about 1 μ m.

CLEM has been used before for autophagy visualization and first commercial implementations are offered. Most CLEM protocols are not optimal for plant research. Marion et al. [38] describe a CLEM workflow on *Arabidopsis* roots observing autophagosomes. They prove how direct CLEM can assist in achieving a superposition of fluorescence signal and ultrastructure, which was helpful with our intermediate step. They conclude that indirect CLEM (voluminous imaging of the sample in a living stage and correlation with the same fixed sample) is not yet feasible and still needs substantial improvement. In our opinion, SPIM is a good method for indirect CLEM as it acquires the whole volume of the root quickly which leaves enough time to HPF it with the same autophagosomes seen during SPIM acquisition. Further assistance in method development was found in publications by Reipert et al. and Kukulski et al. [37], [40], where detailed protocols for HPF and preservation of fluorescence are described, even though the samples they observed were not roots.

Our approach brings live imaging into play, which makes correlation a much bigger challenge and places the correlative workflow at the forefront of method development in multimodal correlative imaging. For more insight into highly dynamic processes such as autophagy, it is indispensable to add an imaging modality to the correlative portfolio that allows to examine temporal changes in organelle composition, such as stress-mediated autophagy patterns over longer time periods. Observing large living samples in their native state and correlating morphological and molecular changes with their ultrastructure will bring a long needed method to the scientific community that will open the door to many current challenges and will allow to tackle urgent and fundamental, yet unanswered research question in a holistic and mechanistic manner.

7 Outlook

Even though first correlative multimodal workflows were successfully established and optimized to assess autophagy, further steps still need to be taken, mainly concerning the reproducibility of the workflows. Many roots were lost after the initial steps of the workflow. One of the reasons is the fact that the HPF device is located in another facility as the SDCM and SPIM are. After performing the initial step, the sample needs to be moved quickly to the high-pressure freezer and placed in the carrier. The time pressure often resulted in removing the root from the gel or coverslip unsuccessfully. Besides, to correlate the modalities directly and with high precision, correlation software will be necessary. As a start, the advanced software included in the Leica CLEM system called Matrix can be used. It is described in detail by Schorb and Sieckmann [41]. The CLEM workflow could be further improved by using another resin that provides better preservation of fluorescence. A paper by Marion et al [38] suggests using glycol methacryl (GMA) as it maintains 5% of water in the sample while it is being embedded. We also plan to use the software *Amira*, as soon as μ CT data will be of satisfying quality. One thing is for certain - our motto will remain: Keep on imaging!

8 Bibliography

- [1] L. W. McDonald and T. L. Hayes, "Correlation of scanning electron microscope and light microscope images of individual cells in human blood and blood clots.," *Exp. Mol. Pathol.*, vol. 10, no. 2, pp. 186–98, Apr. 1969.
- [2] H. D. Geissinger, "A precise stage arrangement for correlative microscopy for specimens mounted on glass slides, stubs or EM grids," *J. Microsc.*, vol. 100, no. 1, pp. 113–117, 1974.
- [3] J. G. White, W. B. Amos, and M. Fordham, "An evaluation of confocal versus conventional imaging of biological structures by fluorescence light microscopy.," *J. Cell Biol.*, vol. 105, no. 1, pp. 41–8, Jul. 1987.
- [4] J. B. Pawley, Ed., *Handbook Of Biological Confocal Microscopy*. Boston, MA: Springer US, 2006.
- [5] D. B. Murphy and M. W. Davidson, "Fundamentals of Light Microscopy and Electronic Imaging," in *Shock*, vol. 17, no. 5, Hoboken, NJ, USA: John Wiley & Sons, Inc., 2012, pp. 267–305.
- [6] Andor an Oxford Instruments company, "Spinning Disk Confocal." [Online]. Available: <http://www.andor.com/learning-academy/spinning-disk-confocal-a-technical-overview>.
- [7] S. J. Wright and D. J. Wright, "Introduction to confocal microscopy.," *Methods Cell Biol.*, vol. 70, pp. 1–85, 2002.
- [8] D. R. Sisan, R. Arevalo, C. Graves, R. McAllister, and J. S. Urbach, "Spatially resolved fluorescence correlation spectroscopy using a spinning disk confocal microscope.," *Biophys. J.*, vol. 91, no. 11, pp. 4241–52, Dec. 2006.
- [9] H. Siedentopf and R. Zsigmondy, "Über Sichtbarmachung und Größenbestimmung ultramikroskopischer Teilchen, mit besonderer Anwendung auf Goldrubingläser," *Ann. Phys.*, vol.

- 315, no. 1, pp. 1–39, 1902.
- [10] J. Huisken, J. Swoger, F. Del Bene, J. Wittbrodt, and E. H. K. Stelzer, “Optical sectioning deep inside live embryos by selective plane illumination microscopy.,” *Science*, vol. 305, no. 5686, pp. 1007–9, Aug. 2004.
- [11] J. Swoger, F. Pampaloni, and E. H. K. Stelzer, “Light-sheet-based fluorescence microscopy for three-dimensional imaging of biological samples.,” *Cold Spring Harb. Protoc.*, vol. 2014, no. 1, pp. 1–8, 2014.
- [12] M. Weber, M. Mickoleit, and J. Huisken, “Light sheet microscopy.,” *Methods Cell Biol.*, vol. 123, pp. 193–215, 2014.
- [13] J. C. Elliott and S. D. Dover, “X-ray microtomography.,” *J. Microsc.*, vol. 126, no. Pt 2, pp. 211–3, May 1982.
- [14] L. A. Feldkamp, S. A. Goldstein, A. M. Parfitt, G. Jesion, and M. Kleerekoper, “The direct examination of three-dimensional bone architecture in vitro by computed tomography.,” *J. Bone Miner. Res.*, vol. 4, no. 1, pp. 3–11, Feb. 1989.
- [15] J. D. Boerckel, D. E. Mason, A. M. McDermott, and E. Alsberg, “Microcomputed tomography: approaches and applications in bioengineering.,” *Stem Cell Res. Ther.*, vol. 5, no. 6, p. 144, Dec. 2014.
- [16] M. Knoll and E. Ruska, “Das Elektronenmikroskop,” *Zeitschrift fuer Phys.*, vol. 78, no. 5–6, pp. 318–339, May 1932.
- [17] D. B. Williams and C. B. Carter, *Transmission Electron Microscopy*. Boston, MA: Springer US, 2009.
- [18] J. Vonck and D. J. Mills, “Advances in high-resolution cryo-EM of oligomeric enzymes,” *Curr. Opin. Struct. Biol.*, vol. 46, pp. 48–54, Oct. 2017.
- [19] University of Liverpool, “Introduction To Electron Microscopes - Transmission Electron Microscope (TEM).” [Online]. Available:

<http://www.materials.ac.uk/elearning/matter/IntroductionToElectronMicroscopes/TEM/index.html>.

- [20] K. Keuenhof, "Preparation of biological specimens for transmission electron microscopy - comparison between chemical fixation and high-pressure freezing," TU Wien, 2017.
- [21] FEI Company, *An Introduction to Electron Microscopy booklet*. .
- [22] Y. Su, M. Nykanen, K. A. Jahn, R. Whan, L. Cantrill, L. L. Soon, K. R. Ratinac, and F. Braet, "Multi-dimensional correlative imaging of subcellular events: Combining the strengths of light and electron microscopy," *Biophys. Rev.*, vol. 2, no. 3, pp. 121–135, 2010.
- [23] P. de Boer, J. P. Hoogenboom, and B. N. G. Giepmans, "Correlated light and electron microscopy: ultrastructure lights up!," *Nat. Methods*, vol. 12, no. 6, pp. 503–13, Jun. 2015.
- [24] I. Hurbain and M. Sachse, "The future is cold: cryo-preparation methods for transmission electron microscopy of cells," *Biol. Cell*, vol. 103, no. 9, pp. 405–420, 2011.
- [25] A. Cavalier, B. M. Humbel, and F. Group, *Cryo-Preparation Methods for Electron Microscopy*. .
- [26] H. Moor and U. Riehle, "Snap freezing under high pressure: a new fixation technique for freeze-etching," in *Proceedings of the 4th European Regional Conference on Electron Microscopy, Rome, 1968*, 1968, vol. 2, pp. 445–446.
- [27] H. Kanno, R. J. Speedy, and C. A. Angell, "Supercooling of Water to -92 C Under Pressure," *Science (80-)*, vol. 189, no. 4206, pp. 880–881, Sep. 1975.
- [28] W. L. Simpson, "An experimental analysis of the Altmann technic of freezing-drying," *Anat. Rec.*, vol. 80, no. 2, pp. 173–189, Jun. 1941.
- [29] H. FERNANDEZ-MORAN, "Low-temperature preparation

- techniques for electron microscopy of biological specimens based on rapid freezing with liquid helium II.," *Ann. N. Y. Acad. Sci.*, vol. 85, no. 2, pp. 689–713, 1960.
- [30] B. M. Humbel and H. Schwarz, "Freeze-substitution for immunochemistry," *Immuno-gold labeling in cell biology*. p. 115, 1989.
- [31] J. H. Hurley and B. A. Schulman, "Review Atomistic Autophagy : The Structures of Cellular Self-Digestion," *Cell*, vol. 157, no. 2, pp. 300–311, 2014.
- [32] P. Boya, F. Reggiori, and P. Codogno, "Emerging regulation and functions of autophagy.," *Nat. Cell Biol.*, vol. 15, no. 7, pp. 713–20, Jul. 2013.
- [33] K. R. Parzych and D. J. Klionsky, "An Overview of Autophagy: Morphology, Mechanism, and Regulation," *Antioxid. Redox Signal.*, vol. 20, no. 3, pp. 460–473, 2014.
- [34] X. Zhuang, H. Wang, S. K. Lam, C. Gao, X. Wang, Y. Cai, and L. Jiang, "A BAR-Domain Protein SH3P2, Which Binds to Phosphatidylinositol 3-Phosphate and ATG8, Regulates Autophagosome Formation in Arabidopsis," *Plant Cell*, vol. 25, no. 11, pp. 4596–4615, 2013.
- [35] R. S. Marshall and R. D. Vierstra, "Autophagy: The Master of Bulk and Selective Recycling," *Annu. Rev. Plant Biol.*, vol. 69, no. 1, p. annurev-arplant-042817-040606, Apr. 2018.
- [36] S. Michaeli and G. Galili, "Degradation of organelles or specific organelle components via selective autophagy in plant cells," *Int. J. Mol. Sci.*, vol. 15, no. 5, pp. 7624–7638, 2014.
- [37] S. Reipert and G. Wiche, "High-pressure freezing and low-temperature fixation of cell monolayers grown on sapphire coverslips.," *Methods Cell Biol.*, vol. 88, pp. 165–80, 2008.
- [38] J. Marion, R. Le Bars, B. Satiat-Jeunemaitre, and C. Boulogne,

- “Optimizing CLEM protocols for plants cells: GMA embedding and cryosections as alternatives for preservation of GFP fluorescence in Arabidopsis roots.,” *J. Struct. Biol.*, vol. 198, no. 3, pp. 196–202, 2017.
- [39] S. Handschuh, N. Baeumler, T. Schwaha, and B. Ruthensteiner, “A correlative approach for combining microCT, light and transmission electron microscopy in a single 3D scenario,” *Front. Zool.*, vol. 10, no. 1, pp. 1–16, 2013.
- [40] W. Kukulski, M. Schorb, S. Welsch, A. Picco, M. Kaksonen, and J. A. G. Briggs, *Precise, Correlated Fluorescence Microscopy and Electron Tomography of Lowicryl Sections Using Fluorescent Fiducial Markers*, vol. 111. Elsevier, 2012.
- [41] M. Schorb and F. Sieckmann, “Matrix MAPS-an intuitive software to acquire, analyze, and annotate light microscopy data for CLEM.,” *Methods Cell Biol.*, vol. 140, pp. 321–333, 2017.